J. Indian Inst. Sci., Jan.–Feb. 1993, **73**, 101–161

IISc THESES ABSTRACTS

Thesis Abstract (Ph.D.)

X-ray crystallographic studies on the effect of chirality on amino acid aggregation by Jayashree Soman.
Research supervisor: M. Vijayan.
Department: Molecular Biophysics Unit.

1. Introduction

A programme of systematic X-ray studies on crystalline complexes involving amino acids and peptides is currently under way in this laboratory[1]. These studies, apart from providing a wealth of information on non-covalent interactions which play a crucial role in the structure, function and assembly of proteins, have resulted in a detailed understanding of different well-defined patterns of amino acid and peptide aggregation. In particular, it has been shown that head-to-tail sequences, in which the α- or terminal amino and carboxylate groups are brought into periodic hydrogen-bonded proximity in a polypeptide-like arrangement, are an almost universal feature of amino acid and peptide aggregation. These sequences assume characteristic geometries and could form the basis for predicting crystalline patterns. These patterns have been shown to be such as to facilitate non-enzymatic condensation into peptides during chemical evolution. Chirality is another factor that needs to be taken into account in studies on chemical evolution and the work reported here is particularly concerned with the effect of chirality on amino acid aggregation and its possible relevance to chemical evolution. Although the X-ray analysis of two binary complexes containing amino acids of mixed chirality, namely, L-arginine D-glutamate trihydrate and L-arginine D-aspartate has provided interesting insights into the effects of charility on molecular aggregation[2], more complexes involving D as well as L amino acids need to be analysed before firm conclusions can be drawn regarding chiral effects. Therefore, a detailed study of crystalline complexes involving amino acids of mixed chirality was taken up.

2. Experimental

A crucial, and at times difficult, step in the X-ray studies on crystalline complexes is the preparation of suitable single crystals. Through extensive crystallisation experiments, crystals of the following complexes suitable for X-ray studies could be grown: 1. L-lysine D-glutamate, 2. L-lysine D-aspartate monohydrate, 3. L-ornithine D-aspartate, 4. A new form of L-arginine D-glutamate, 5. DL-arginine DL-glutamate monohydrate, 6. DL-arginine DL-aspartate, 7. DL-arginine acetate monohydrate, and 8. DL-lysine acetate. The space group and the unit cell dimensions of the crystals were determined using X-ray diffraction photographs. The cell parameters were subsequently refined on a CAD-4 computer-controlled diffractometer. X-ray intensity data were collected on the diffractometer using nickel-filtered copper radiation or monochromated molybdenum radiation. All the structures were solved using direct methods employing MULTAN or SHELX. Atomic parameters were refined using the full matrix structure factor least-squares method.

3. Results and discussion

The lysine molecule in L-lysine D-glutamate[3] assumes a conformation with the side chain staggered between the α-amino and the α-carboxylate groups. The molecular aggregation is very similar to that in

L-arginine D-aspartate and L-arginine D-glutamate trihydrate[2]. The molecules arrange themselves as double layers. The core of each double layer consists of two parallel sheets, each involving both types of molecules. The hydrogen bonds within each sheet and those that connect the two sheets give rise to LL-, DD- and DL-type head-to-tail sequences. Adjacent double layers are held together by side chain–side chain interactions. In contrast, the unlike molecules in L-lysine D-aspartate monohydrate[3] aggregate into separate alternating layers as in the case of most LL complexes. The arrangement of molecules in the lysine layer is nearly the same as that in L-lysine L-aspartate[4], with head-to-tail sequences as the central feature. The arrangement of aspartate ions in the layers containing them is, however, unusual. The aspartate ions form hydrogen-bonded helical columns around crystallographic 2_1 screw axes. Adjacent aspartate columns are connected through a column of water molecules. The aspartate ions do not take part in head-to-tail sequences. The interactions of the side-chain amino group of lysine in the two complexes are such that they form infinite sequences containing alternating amino and carboxylate groups.

The aggregation pattern in L-ornithine D-aspartate monohydrate[5] is entirely different from that in L-ornithine L-aspartate hemihydrate[6]. It is similar to that in L-lysine D-aspartate monohydrate in that the unlike molecules aggregate into separate alternating layers, but is different from that in the other three LD complexes. The organisation of molecules in the ornithine layer is similar to that in the lysine layer in L-lysine D-aspartate monohydrate, with two head-to-tail sequences stabilising the layer. The arrangement of the aspartate ions, however, is very different from any observed so far in crystal structures containing aspartic acid or aspartate ions. The aspartate layer is made up of molecular ribbons each containing one head-to-tail sequence. Adjacent ribbons are interconnected through water molecules and side chain amino groups. An interesting feature of the structure is an internal water bridge between the α-amino group and one of the side-chain carboxyl oxygen atoms of the aspartate ion. The structure contains a closed hydrogen-bonded loop made up of alternating amino and carboxylate groups.

In terms of composition the new form of L-arginine D-glutamate differs from the old form in that the former is a monohydrate whereas the latter is a trihydrate[2]. The conformation of the arginine molecule is the same in both the forms whereas that of the glutamate ion is different. The change in the conformation of the glutamate ion is such that it facilitates extensive pseudosymmetry in the new form. The molecules arrange themselves in double layers stabilised by head-to-tail sequences, in both the forms. However, considerable differences exist between the two forms in the interface, consisting of side chains and water molecules, between double layers. A comparative study of the relationship between the crystal structures of L and DL amino acids on the one hand and that between the structures of LL and LD amino acid–amino acid complexes on the other, leads to some interesting observations[7]. The crystal structures of most hydrophobic amino acids are made up of double layers and those of most hydrophilic amino acids contain single layers irrespective of the chiralities of the amino acids involved. In most cases, the molecules tend to appropriately rearrange themselves to preserve the broad features of aggregation patterns when the chirality of half the molecules is reversed as in the structures of DL amino acids. The basic elements of aggregation in the LL and the LD complexes are similar to those found in the crystals of L and DL amino acids. However, the differences between the LL and the LD complexes in the distribution of these elements are more pronounced than those between the distributions in the structures of L and DL amino acids.

The aggregation patterns in the crystal structures of DL-arginine DL-glutamate monohydrate and DL-arginine DL-aspartate, the first DL–DL amino acid–amino acid complexes to be prepared and X-ray analysed[8], can be described in terms of two-dimensional patterns, but unlike in the case of most LL and LD complexes these patterns do not involve head-to-tail sequences. The basic element of aggregation in both the structures is an infinite chain made up of pairs of molecules. Each pair, consisting of an L and a D isomer, is stabilised by two centrosymmetrically or nearly centrosymmetrically related hydrogen bonds involving the α-amino and the α-carboxylate groups. Adjacent pairs in the chain are then connected by specific guanidyl-carboxylate interactions. The infinite chains are interconnected through hydrogen bonds to form molecular sheets. The sheets are then stacked along the shortest cell translation. The interactions between sheets involve two head-to-tail sequences in the glutamate complex and one such sequence in the aspartate complex. Thus, fundamental differences exist among the aggregation patterns in the LL, the LD and the DL–DL complexes. The differences are such that if condensation were to take place in the different aggregates, the LL aggregate is more likely to yield clean peptide fragments than the other two.

Acetic acid is one of the compounds produced in simulated prebiotic synthetic experiments and a study of its interactions with amino acids is of interest in relation to chemical evolution. A comparison of the crystal structures of DL-arginine acetate monohydrate and DL-lysine acetate[9] with the corresponding L amino acid–acetate complexes that have already been analysed[10,11] provide insights into the effect of chirality on molecular aggregation. The basic elements of aggregation in both the structures are pairs of amino acid molecules, each pair stabilised by two centrosymmetrically related hydrogen bonds involving α-amino and α-carboxylate groups, stacked along the shortest dimension to form columns. The pairs are held together in each column by head-to-tail sequences. The columns stack along a crystallographic axis to form layers. Adjacent layers are bridged by acetate ions. The amino acid–acetate interactions are primarily through side chains and involve specific interactions and characteristic interaction patterns. The gross features of molecular aggregation are nearly the same in DL-arginine acetate and L-arginine acetate whereas they are substantially different in the lysine complexes. As in the L-amino acid–acetate complexes, electrostatic effects are modulated by other factors to give rise to head-to-tail sequences in the present structures also. In both the cases, one of the two head-to-tail sequences in the L complex is replaced by a hydrogen-bonded loop involving α-amino and α-carboxylate groups in the DL complex. This may have implications for prebiotic condensation during chemical evolution

References

1. VIJAYAN, M. — *Prog. Biophys. Mol. Biol.*, 1988, **52**, 71–79
2. SURESH, C. G., RAMASWAMY, J. AND VIJAYAN, M — *Acta Crystallogr B*, 1986, **42**, 473–478.
3. SOMAN, J., SURESH, C G. AND VIJAYAN, M — *Int J. Peptide Protein Res* , 1988, **32**, 352–360
4. BHAT, T. N AND VIJAYAN, M. — *Acta Crystallogr. B*, 1976, **32**, 891–895.
5. SOMAN, J. AND VIJAYAN, M. — *Acta Crystallogr. C*, 1988, **44**, 1794–1797.
6 SALUNKE, D. M. AND VIJAYAN, M. — *Int J. Peptide Protein Res.*, 1983, **22**, 154–160.
7. SOMAN, J. AND VIJAYAN, M. — *J. Biosci* , 1989, **14**, 111–125.
8 SOMAN, J., VIJAYAN, M., RAMAKRISHNAN, B. AND GURU ROW, T. N. — *Biopolymers*, 1990, **29**, 533–542.
9. SOMAN, J., RAO, T , RADHAKRISHNAN, R. AND VIJAYAN, M. — *J Biomol. Struct. Dynamics*, 1989, **7**, 269–277
10. SURESH, C G. AND VIJAYAN, M. — *Int. J. Peptide Protein Res.*, 1983, **21**, 223–226.
11. SURESH, C. G. AND VIJAYAN, M. — *Int. J. Peptide Protein Res* , 1983, **22**, 617–621

Thesis Abstract (Ph.D.)

Small molecules of biological and chemical interest: X-ray crystallographic studies and space group frequency analysis by N. Padmaja.
Research supervisors: S. Ramakumar and M. A. Viswamitra.
Department: Physics.

1. Introduction

Crystallographic studies in the past have provided considerable information on aspects of conformational features and molecular interactions of nucleic acid constituents. Five of the eight compounds whose crystal

structures are reported in the work have been taken up in this connection. Three of these relate to nucleic acid constituents with a biologically relevant modification of methylation of cytosine and adenine bases. The remaining two structures are of model compounds chosen to examine certain elementary patterns of interactions which could be of significance to a wider problem of protein–nucleic acid interactions.

X-ray analysis has also been carried out on three heterocyclic compounds with bulky substituents which are chosen particularly to study the effect of substituents on the conformation of the overcrowded central ring.

Studies relating to the theoretical aspects have also been initiated with a problem of relevance to the molecular packing in crystals. Space group frequency distributions for organic small molecule crystal structures as well as for protein crystal structures have been computed and some interesting observations have been made.

2. Experimental studies

The crystals of the nucleic acid-related constituents reported in the work were all crystallized by evaporation techniques. The intensity data for the crystals were collected on a CAD-4 Enraf–Nonius diffractometer. The Enraf–Nonius Structure Determination Package was used for structure solution. The data required for the space group frequency analysis was extracted from the Cambridge Structural Database and Protein Data Bank, Brookhaven.

3. Main results and discussion

Crystal structure analysis has been carried out on two cytosine compounds, 5-methylcytosine HCl and 5-methylcytidine[1, 2], which carry a biologically relevant modification of 5-methylation. A detailed analysis of 5-methylated cytosine structures in comparison with their unmethylated analogues has shown that methylation affects the molecular dimensions of bases, with a tendency of reduced base stacking in methylated cytosine structures. The results obtained here significantly add to the original contributions relating to the effects of protonation and halogenation[3, 4]. Interestingly, it is found that the modified adenosine structure, puromycin aminonucleoside (reported in the thesis), which contains an N6-dimethylated adenine, showed the involvement of the methyl groups in the base-stacking interactions. The compound being a derivative of puromycin, a broad spectrum antibiotic that inhibits protein synthesis, has been useful in obtaining some clues as to where exactly the conformational flexibility of its parent molecule comes from—its nucleoside portion or its amino acid segment. With the conformation of the present structure [*anti*, C(3′)-*endo*-C(2′)-*exo*, O(5′) atom disordered between *gauche-trans* and *gauche-gauche* orientations] being essentially similar to that of the nucleoside portion of the parent molecule puromycin[5] [*anti*, C(3′)-*endo*-C(2′)-*exo*, *gauche-gauche*], it is felt that the conformational flexibility of puromycin does not seem to come from its nucleoside segment, but could possibly lie in its amino acid part.

The study on model compounds, 2′-O-monosuccinyl adenosine 3′,5′-(cyclic) phosphate monohydrate[6] and 5′-O-monosuccinyl adenosine dihydrate, has shown that the succinic acid moiety which resembles the side chain of glutamic acid, binds through direct and water-mediated interactions to the adenine base. The interaction patterns found here have been rather new considering the interactions between similar groups in structures of related compounds. Interestingly, somewhat similar type of water-mediated interactions found in the cAMP derivative here, has indeed been noticed in certain DNA operator–repressor protein complexes. Another most exciting observation comes from the adenosine derivative. A near-perpendicular approach of adenine base crosslinking a stacked pair of adenine bases has been an interesting feature in view of the normally found inplane or skewed approaches of bases in nucleoside, nucleotide and polynucleotide structures and it seems to open up possibilities for generating novel nucleic acid structures.

X-ray studies have been carried out on the following three heterocyclic compounds, in view of the intrinsic chemical and conformational interest in such overcrowded molecules:

3-Ethyl-2,6-diphenyl-N-benzoyl piperidin-4-one,
3-Ethyl-2,6-diphenyl-N-phenylcarbamoyl piperidin-4-one, and
3-Methyl-2,7-diphenyl-N-phenylcarbamoyl-hexahydro-1,4-diazepin-5-one.

Among the several points of interest, it is worth noting the conformational flexibility exhibited by the heterocyclic ring of the piperidine derivatives, carrying similar substituents, which takes up a *twist-boat* form in one and a *distorted boat* form in the other.

As stated earher, the thesis also reports a statistical problem of relevance to the molecular packing in crystals. In this connection, the space group frequencies of organic small molecules crystallized with more than one formula unit in the asymmetric unit have been calculated. The distribution has been observed to be different from that for the case where all compounds in the Cambridge Structural Database are considered. Statistics have shown that lower symmetry space groups are more preferred when more than one formula unit per asymmetric unit are present[7].

The calculations were extended to macromolecular crystal structures and the space group frequencies of proteins, which are chiral in nature, have thus been computed. The distribution for proteins in the 65 possible space groups, which do not have operations of second kind, when compared with that for small molecules in these space groups belonging to the tetragonal and trigonal crystal systems, is distinctly more than that for small molecules. It is felt that this could arise owing to the protein subunit aggregation which is expected to give more regular shapes to proteins, thus allowing them to pack with higher symmetries.

References

1. PADMAJA, N., RAMAKUMAR, S. AND VISWAMITRA, M. A. — *Acta Crystallogr. C*, 1987, **43**, 2157–2160
2. PADMAJA, N., RAMAKUMAR, S AND VISWAMITRA, M. A. — *Acta Crystallogr. C*, 1991, **47**, 1445–1448.
3. BUGG, C. E., THOMAS, J M., SUNDARALINGAM, M. AND RAO, S. T — *Biopolymers*, 1971, **10**, 175–219.
4. MUKHTAR, J. H N. AND WILSON, H R. — *Acta Crystallogr B*, 1978, **34**, 337–339.
5. SUNDARALINGAM, M. AND ARORA, S. K. — *J. Mol. Biol.*, 1972, **71**, 49–70
6. PADMAJA, N., RAMAKUMAR, S. AND VISWAMITRA, M. A. — *Bull. Chem Soc. Jap.*, 1991, **64**, 1359–1363.
7. PADMAJA, N., RAMAKUMAR, S. AND VISWAMITRA, M. A — *Acta Crystallogr. A*, 1990, **46**, 725–730.

Thesis Abstract (Ph.D.)

Studies on riboflavin carrier protein: Isolation and hormonal modulation of its biosynthesis in the mammary gland and characteristics of its placental receptor by P. Devi Prasad.

Research supervisor: P. R. Adiga.

Department: Biochemistry.

1. Introduction

Earlier investigations in this laboratory have emphasized the important function played by the riboflavin carrier protein (RCP) in the transplacental delivery of riboflavin across the placental barrier to the fetus. The role of this protein in fetal nutrition is demonstrated by experiments wherein immunoneutralization of endogenous RCP in female rats by antibodies to chicken egg RCP leads to fetal wastage and termination of pregnancy[1]. The mammals' neonate is still dependent on the mother for its nutritional requirement and there should be built-in mechanisms to ensure adequate vitamin supply in the form of milk. In addition, the presence of high amounts of riboflavin in milk prompted the present investigations leading to identifi-

cation of RCP in milk, its isolation from bovine milk and its biosynthesis and hormonal modulation in the rat mammary gland.

The envisaged function for RCP in fetal vitamin nutrition requires that a RCP-specific receptor be present on the placental membranes. Part II of the work deals with the identification and characterization of such a receptor in the human term placenta for the first time.

2. Experimental procedures

RCP was detected in the milk whey of different species by a specific radioimmunoassay (RIA). RCP from bovine milk was purified by treatment with EDTA to break the Ca^{2+} bridges between phosphoproteins, acid precipitation of caseins followed by chromatography on DEAE–cellulose, affinity chromatography on riboflavin affinity matrix and finally on Mono Q column using FPLC. The immunological characterization of the purified protein was achieved by RIA, Western blotting and immunoprecipitation using specific polyclonal and monoclonal antibodies (MAbs). Two-dimensional tryptic peptide analysis was done according to the method of Elder *et al*[2]. Immunohistochemical localization of RCP on mammary tissue sections was carried out using peroxidase conjugate and diamino benzidine. (cRCP-specific cDNA was a gift from Dr. H. B. White, University of Delaware, Newark, Delaware). Isolation of total RNA from various tissues and Northern analysis of the isolated total RNA was performed as detailed in Maniatis *et al*[3]. *In situ* hybridization of RCP–RNA was carried out on paraffin sections using ^{32}P-labelled cRCP–cDNA. Following hybridization, the sections were washed under stringent conditions and coated with Kodak NTB3 emulsion The hormonal modulation of RCP-mRNA in the rat mammary gland was studied by monitoring the RCP-mRNA levels under physiological conditions and by injecting pharmacological doses of different hormones.

For placental receptor characterization crude placental membrane was prepared[4] and enriched syncytiotrophoblast membrane was isolated[5]. Standard binding assay was performed in 1·5-ml plastic tubes containing 400–600 μg of membrane protein, 150 mM Na–K phosphate buffer pH 6·8, 0·15-mg bovine serum albumin, 2 mM MgCl, 1 mM phenyl methyl sulfonyl fluoride and 200,000 cpm of ^{125}I-labelled RCP in a total volume of 100 μl. The reaction mixture was incubated for 30 min at 30°C and then the bound ligand was separated from the free by filtering through siliconized GF/C filters. Inhibition studies with various chemically modified RCPs were done by coincubation of the modified ligand, radioiodinated RCP and the receptor. Inhibition studies with different MAbs were carried out by pre-incubating the individual MAb with the radioiodinated ligand for 16 h at 4° followed by incubation with the membrane for 30 min at 30°C.

3. Results and discussion

One of the major highlights of the present study is the unequivocal demonstration for the first time that RCP which obligatorily participates in transplacental vitamin transport during gestation in mammals is a definite protein constituent of the milk of various mammalian species from rodents to humans and exhibits gross physicochemical and immunological similarities to its chicken-egg white counterpart.

By employing a sensitive heterologous RIA, immunologically homologous RCP was detected in the milks of several mammalian species. RCP was purified to homogeneity from bovine milk by a three-step procedure. The high degree of enrichment of RCP involving riboflavin epoxy Sepharose affinity chromatography showed that the immunologically cross-reacting protein binds riboflavin with high affinity. The purified cross-reacting protein and an approximate M_r of 35 ± 2 K and bound to all the MAbs except to 6B2C12 which recognizes the C-terminal tail end of the cRCP. This suggests that the RCP isolated from the bovine milk is lacking the sequential epitope located at the C-terminal end of the chicken RCP. This high degree of immunological similarity between the bovine milk and the chicken RCP could be further corroborated by their similar two-dimensional tryptic peptide maps. Preliminary evidence for the synthesis of RCP in the mammary gland was provided by immunohistochemical localization of the vitamin carrier in the lactating rat mammary gland. This is further supported by the demonstration of the RCP-specific mRNA in both pregnant and lactating rat mammary gland as measured by Northern blot analysis. A strong signal with a size approximately of 1 kb, *i.e.*, similar to that of chicken RCP–mRNA clearly indicates

the extensive sequence homology between the two proteins. The proof for the RCP–mRNA capable of being translated in both pregnant and lactating mammary glands stems from studies involving immunoprecipitation of *in vitro* [^{35}S]-methionine-labelled protein. Further, *in situ* hybridization of cytoplasmic RNA with [^{32}P]-labelled chicken RCP–cDNA showed that the mammary acinar cells are the major cell type involved in the elaboration of RCP.

It has been earlier established that the biosynthesis of RCPs in the chicken and mammals including primates are estrogen modulated. Higher levels of RCP–mRNA encountered during diestrous stage, albeit marginal, indicated that the RCP in the mammary gland may also be modulated by estrogen. The RCP–mRNA levels in the pregnant as well as lactating rat mammary glands were also shown to fluctuate in concert with the estrogen levels being highest during mid gestation and lactation.

Conclusive proof for mammary RCP as an estrogen-inducible gene product was obtained by administration of pharmacological doses of the sex steroid to both mature and immature female rats. Estrogen was shown to stimulate RCP gene expression at very low concentration (0·1 mg/kg body wt). Following steroid administration at a pharmacological dose, high levels of RCP–mRNA were encountered at 12 h which remains continuously elevated up to 72 h. Progesterone was also effective in stimulating the RCP gene, but exhibited different time course of response. The specificity of the progesterone induction was deduced by using TMX, an antiestrogen which completely curtailed the estrogenic response but could only partly inhibit the progesterone-induced RCP gene expression. Though further experimentation is warranted, the data presented strongly suggest that the sex steroids, estrogen and progesterone, are the primary modulators of RCP gene expression in the mammary tissue.

In summary, the results presented in Part I of the work clearly reveal for the first time that the highly evolutionarily conserved RCP is present in the milk of all species of mammals tested. It would thus appear that RCP is also involved in neonatal nutrition in addition to playing a major role in fetal vitamin nutrition. The finding that in the mature mammary gland both estrogen and progesterone can stimulate RCP gene expression strongly suggest that the factors regulating RCP gene expression in mammary tissue are similar to that in the avian and mammalian liver.

Towards identification and characterization of RCP-specific receptors on human-term placental membranes, a heterologous radio-receptor assay (RRA) using ^{125}I-labelled chicken egg white RCP as the ligand was standardized In analogy, with other ligand–receptor systems, the binding reaction was clearly dependent on time, temperature and the amount of membrane protein and ligand concentration in the assay system. Further, Mg^{2+} at a final concentration of 2 mM was very essential for the ligand–receptor interaction. Some of the structural features of RCP involved in its interaction with the receptor were elucidated. Dephosphorylated and deglycosylated RCP failed to inhibit the binding of ^{125}I-labelled RCP to the receptor and yolk RCP, which lacks the C-terminal tail of the molecule, but partially inhibits the binding of the radioiodinated egg white RCP to the receptor. Thus, it appears that the bound phosphate, the carbohydrate side chains and the C-terminal tail of the molecule are involved in the receptor interaction. Additionally, evidence for the involvement of the peptidyl backbone in receptor binding was obtained. From the finding that MAb 6B2C12 which binds to the C-terminal tail of RCP significantly inhibited the ligand receptor interaction focuses on the importance of this region of RCP in receptor binding. This contrasts with the observation that MAb 6H10F7 though bound the ligand with high affinity fails to curtail the ligand–receptor interaction. Since other MAbs also inhibited the ligand–receptor interaction to different extents, it would appear that the RCP–receptor interaction is complex involving multiple interacting sites. Thus, the results detailed in Part II conclusively prove the presence of RCP-specific receptor on the human placental membranes. In addition, the importance of carbohydrate side chain, phosphoserine moieties and C-terminal tail of the ligand in receptor binding has been emphasized.

References

1. ADIGA, P. R., VISWESWARIAH, S. S., KARANDE, A. A. AND KUZHANDHAIVELU, N. — *J. Biosci.*, 1988, **13**, 87–104.

2. ELDER, J. H., PICKETT, R. A. II, HAMPTON, J. AND LERNER, R. A. — *J. Biol. Chem.*, 1977, **252**, 6510–6515.

3 MANIATIS, T., FRITSCH, E F. AND SAMBROOK, J. — In *Molecular cloning* (T. Maniatis, E F. Fritsch and J. Sambrook, eds), p 190, 1982, Cold Spring Harbor Laboratory, Cold Spring Harbor, NY.

4 CURRIE, A J., FRASER, H. M. AND SHARPE, R M — *Biochem Biophys Res Commun*, 1981, **99**, 332–338.

5. SMITH, C H., NELSON, D M., KING, B F., DONOHUE, T. M., RUZYCKI, S. M. AND KELLEY, I. K — *Am J Obstet Gynec.*, 1977, **128**, 190–196

Thesis Abstract (Ph.D.)

Immunochemical studies on riboflavin carrier protein by N. Kuzhandhaivelu.
Research supervisor: P. R. Adiga.
Department: Biochemsitry.

1. Introduction

Riboflavin carrier proteins (RCP) having extensive immunological and physicochemical similarities with that of chicken RCP have been identified earlier in this laboratory in various mammalian species including primates (also humans)[1,2]. The vital role of this protein in transplacental flavin transport during gestation in rats and monkeys was established by experiments wherein immuno-neutralization of RCP in female rats[3] and monkeys[4] by antibodies to chicken RCP led to fetal wastage and early termination of pregnancy. These results prompted the investigation detailed in the present molecular immunological studies employing monoclonal antibodies (MAbs) raised to chicken RCP.

2. Experimental procedures

Monoclonal antibodies were raised to chicken egg apo-RCP by the Kohler and Milstein's hybridoma technology[5]. This resulted in a panel of 18 stable, high-affinity, IgG-secreting clones. To localise the peptidyl sequences recognized by some of these MAbs, MAbs were probed with either peptide fragments isolated from RCP or with synthetic peptide based on the primary structure of RCP. MAbs were used to study the reconstitution of the epitopes during refolding of disulphide reduced and unfolded RCP on determinant-to-determinant basis.

3. Results and discussion

Based on the pattern of competitive inhibition of binding of the ^{125}I-labelled MAbs to RCP in the presence of individual unlabelled MAbs in solid-phase radioimmunoassay (RIA), the 18 clones obtained were divided into seven sub-groups each recognizing a single epitope. One representative clone from each subgroup was propagated for further detailed analysis and were termed as 6A4D7, 6B2C12, 5A2E6, 6H10F7, 5B1D3, 5C4C6 and 5G1E11 MAbs. The conservation of epitopes recognized by the MAbs was analysed in partially purified RCPs from the pregnancy sera of rat, cow and human. Except for the absence of the epitope recognized by 5G1E11 MAb in the RCP from cow, all other epitopes were found to be conserved in RCPs present in the mammalian species investigated. A C-terminal 133 amino-acid polypeptide isolated from 75% formic acid digest of RCP was found to react with a minimum of 3 MAbs, *viz.*, 6B2C12, 5B1D3 and 5A2E6 as analysed by solid-phase RIA. A phosphopeptide comprising 182–204 amino acid sequence and harbouring all the 8 phosphoserine residues on RCP isolated from tryptic digest of reduced and carboxymethylated RCP (RCM–RCP) was found to selectively recognize the 5B1D3 MAb but not others. When the peptidyl sequence of 203–219 amino acid residues present at the extreme C-terminus of RCP was chemically synthesized and probed with all the MAbs, only 6B2C12 MAb specifically recognized this peptide in both solid- and liquid-phase RIAs. An attempt was made to delineate the most crucial MAb recognizable epitope involved in curtailing, due to immunoblockade of the carrier, the transplacental

riboflavin transport in rodents. When 6B2C12 MAb ascites were administered intraperitoneally to mice with confirmed early pregnancy, there was 100% early embryonic resorption. On the other hand, when similar experiments were carried out using ascites derived from either SP2/0 cell line or 6H10F7 clone, the mice delivered normal pups. Presumably, the RCP-6B2C12 MAb immunecomplex interfered effectively with transplacental flavin transport due to steric blockade of specific surface recognition sites on the vitamin carrier. The optimal *in vitro* conditions for maximal refolding of completely unfolded RCP were standardized. The optimal RCP concentration in the renaturation mixture was found to be 2 mg/ml at pH 8·6 with an optimal temperature at 20°C. The processes of unfolding and refolding of RCP were monitored by determining the number of moles of free sulphydryl group, protein fluorescence spectra (^{14}C)-flavin binding and quenching of flavin fluorescence by the protein, molecular size/shape of the protein by analytical gel filtration chromatography and the mobility of the protein in alkaline PAGE. The unfolded RCP when tested for immunoreactivity in enzyme-linked immunosorbant assay was found to react only with 6B2C12 MAb signalling the presence of a sequential epitope. Once the RCP was folded into its native structure all the conformational epitopes were also reconstituted proving the point that the conformation-specific RCP MAbs are dependent more on the tertiary folding of RCP rather than its local secondary structure.

References

1. ADIGA, P. R. MURTY, C. V. R — Vitamin carrier protein during embryonic development in birds and mammals, in *Molecular biology of egg maturation*, Ciba Foundation Symposium 98, pp 111–136, 1983, Pitman.
2. ADIGA, P. R., VISWESWARIAH, S. S. KARANDE, A. A AND KUZHANDHAIVELU, N. — Biochemical and immunological aspects of riboflavin carrier proteins, *J. Biosci.*, 1988, **13**, 87–104.
3. MURTY, C. V. R AND ADIGA, P. R — Pregnancy suppression by active immunization against riboflavin carrier protein, *Science*, 1982, **216**, 191–193.
4. SESHAGIRI, P. B. AND ADIGA, P R — Pregnancy suppression in the bonnet monkey by active immunization with chicken riboflavin carrier protein, *J Reprod. Immun.*, 1987, **12**, 93–107
5. KOHLER, G. AND MILSTEIN, C. — Continuous cultures of fused cells secreting antibody of predefined specificity, *Nature*, 1975, **256**, 495–497.

Thesis Abstract (Ph.D.)

X-ray crystallographic studies on amino acid and peptide complexes of succinic acid

by G. Sridhar Prasad.
Research supervisor: M. Vijayan.
Department: Molecular Biophysics Unit.

1. Introduction

A major research programme in this laboratory is concerned with biomolecular interactions and consists primarily of the preparation and X-ray analysis of crystalline complexes involving amino acids and peptides, among themselves as well as with other molecules[1]. These studies, in addition to providing information on the non-covalent interactions which play a vital role in the structure, function and assembly of proteins, have also resulted in a detailed understanding of well-defined patterns of amino acid and peptide aggregation[2,3]. These patterns with head-to-tail sequences in which the main chain amino and carboxylate groups are brought into hydrogen-bonded proximity in a polypeptide-like arrangement have been shown to be relevant to prebiotic polymerisation during chemical evolution[4]. The effect of chirality on amino acid aggregation has also been explored through the analysis of complexes involving amino acids of mixed chirality[5]. Yet another problem the programme addresses is concerned with the elucidation of specific

interactions and characteristic interaction patterns which might have been important in the self-assembly of primitive multi-molecular systems[1,6,7]. The current focus of the programme is on the complexes of amino acids and peptides with other organic compounds which are believed to have existed in the prebiotic milieu. In this context, complexes involving succinic acid, a compound which is invariably produced in simulated prebiotic experiments and also found in carbon-containing meteorites, are of considerable interest.

2. Experimental

After extensive experimentation involving the variation of parameters such as concentration, stoichiometry and precipitant, single crystals of the complexes of succinic acid with DL- and L-arginine, DL- and L-lysine (two forms of the L-lysine complex), DL- and L-histidine, DL-proline and glycyl-L-histidine were prepared by the diffusion of organic liquids into the aqueous solutions of the components. The crystals were characterised using X-ray diffraction photographs and the intensity data from them were collected on a computer-controlled diffractometer. The structures were solved using the direct methods and refined employing the full matrix structure factor least-squares procedure.

3. Results and discussion

On the basis of stiochiometry ionisation state and hydration, the complexes involving DL- and L-arginine[8] may be described as DL-arginine hemisuccinate dihydrate and L-arginine hemisuccinate hemisuccinic acid monohydrate, respectively. Two of the three crystallographically independent arginine molecules in the complexes have conformations different from those observed so far in the crystal structures containing arginine. The crystal structure of the L-arginine complex is highly pseudosymmetric. Arginine–succinate interactions in both the complexes involve specific guanidyl–carboxylate interactions. The basic elements of aggregation in both the structures are ribbons made up of alternating arginine dimers and succinate ions. However, the ribbons pack in different ways in the two structures.

Succinic acid in the crystal structures of the DL-lysine and the two L-lysine complexes[9] exhibit a variety of ionisation states. Two of the lysine conformations found in the complexes have been observed for the first time in crystals containing lysine. Form (II) of the L-lysine complex is highly pseudosymmetric. In all the complexes, unlike molecules aggregate into separate alternating layers. The basic element of aggregation in the lysine layer in the complexes is an S2-type head-to-tail sequence. This element combines in different ways in the three structures. The basic element of aggregation in the succinic acid layer in the complexes is a hydrogen-bonded ribbon. The ribbons are interconnected through amino groups in the lysine layer.

The histidine complexes with succinic acid may be described as DL-histidine hemisuccinate dihydrate and L-histidine semisuccinate trihydrate. In the DL-histidine complex, the amino acid molecules aggregate into double ribbons or columns which then form a layer. The aggregation of histidine and water molecules leaves behind voids which are occupied by succinate ions. In the L-histidine complex, the amino acid molecules form columns; so do the semisuccinate ions and water molecules. The two columns interdigitate to form the complex crystal.

The only neutral amino acid with which a succinic acid complex could be prepared was DL-proline. The proline molecules in the structure aggregate into layers stabilized by DL1 and DL2 head-to-tail sequences. This arrangement is remarkably similar to the aggregation patterns observed in the crystal structures of most (uncomplexed) hydrophobic amino acids. The amino acid layers stack in such a way that the succinic acid molecules are enclosed in the voids left behind.

Crystals could be grown only of one dipeptide complex, namely, glycyl-L-histidine semisuccinate monohydrate. The semisuccinate ions in the structure exhibit considerable departure from planarity. The dipeptide molecules aggregate into layers. The aggregation pattern in the layers is very similar to one of the idealized patterns predicted earlier for L-alanyl-L-alanine. The semisuccinate ions are located in the voids left behind when the amino acid layers aggregate.

A comparison of the nine crystalline complexes provides several interesting insights. The complexes exhibit substantial variability in the ionisation state of the stoichiometry involving succinic acid. This makes an exploration of the possible catalytic role of succinic acid in the prebiotic scenario worthwhile. Succinic acid molecules and succinate ions appear to prefer a planar centrosymmetric conformation with the two carboxyl (carboxylate) groups *trans* with respect to the central C–C bond, although substantial departures from this conformation are possible. The presence of succinic acid gives rise to new patterns of amino acid aggregation. Commonalities, however, exist among groups of succinic acid complexes. Some of the complexes can be described as inclusion compounds with the amino acid/dipeptide as the host and succinic acid/semisuccinate/succinate as the guest. A comparison of the structures involving DL and L isomers of the same amino acid indicates that the effects of change in chirality, though very substantial, are not the same in different pairs of complexes.

References

1	VIJAYAN, M.	*Prog. Biophys. Mol. Biol.*, 1988, **52**, 71–99
2.	SURESH, C. G. AND VIJAYAN, M.	*Int. J. Peptide Protein Res.*, 1983, **22**, 129–143
3.	SURESH, C. G. AND VIJAYAN, M.	*Int. J. Peptide Protein Res.*, 1985, **26**, 311–328
4.	VIJAYAN, M.	*FEBS Lett.*, 1980, **112**, 135–137
5	SOMAN, J., VIJAYAN, M., RAMAKRISHNAN, B. AND GURU ROW, T. N.	*Biopolymers*, 1990, **29**, 533–542
6.	SALUNKE, D. M. AND VIJAYAN, M.	*Int. J. Peptide Protein Res.*, 1981, **18**, 348–351
7	SOMAN, J., SURESH, C. G. AND VIJAYAN, M.	*Int. J. Peptide Protein Res.*, 1988, **32**, 352–360
8	PRASAD, G. S. AND VIJAYAN, M.	*Int. J. Peptide Protein Res.*, 1990, **35**, 357–364
9	PRASAD, G. S. AND VIJAYAN, M.	*Acta Crystallogr. B*, 1991, **47**, 927–935.

Thesis Abstract (Ph.D.)

Structure and interactions of polyamines by S. Ramaswamy.

Research supervisor: Mathur R. N. Murthy.

Department: Molecular Biophysics Unit.

1. Introduction

Polyamines are ubiquitous biological cations. Their high concentration in cells, increase in rapidly growing tissues and the regulatory mechanisms that have evolved for controlling them point to the importance of polyamines in living cells. There is evidence for direct and indirect involvement of polyamines in the regulation of enzymes. It has also been shown that spermine stabilizes ribonuclease T_1 and DNA against thermal denaturation. The crystal structure of the first polyamine salt was published as early as 1949. Yet, structural studies illustrating polyamine interactions are limited. The first structure of a polyamine complexed to an organic molecule, the macrotricycle-II with cadaverine dication was solved only in 1982. Though the structure of phenylalanine-transfer RNA contained two polyamine molecules, the resolution did not permit elucidation of interaction at atomic level. In order to understand the mode of interaction of polyamines with other ubiquitous biomolecules it is necessary to determine structures of polyamines under a variety of biologically relevant chemical contexts. Towards this goal, structural studies on polyamines and their complexes with acidic amino acids were undertaken.

2. Inorganic salts of polyamines

Structures of inorganic salts of polyamines have been useful in modelling polyamine interactions and in

explaining the effect of polyamines on nucleic acid conformation. The structures of the chloride salts of type NH_3^+-$(CH_2)_n$ NH_3^+ for n = 2, 3, 4 and 6 have been determined earlier. However, repeated attempts to determine the structure when n = 5 (cadaverine), made earlier, were unsuccessful. Therefore, determination of the structure of cadaverine dihydrochloride was undertaken. Occasionally, unusual polyamines are found to be present in certain organisms. It has been shown that a homolog of spermidine, symmetrical homospermidine, is the major polyamine in sandal leaves. The determination of the structure of the phosphate salt of sym-homospermidine isolated from sandal leaves provided the opportunity of comparing this structure with its normal homolog.

3. Polyamine complexes

In order to elucidate the nature of polyamine interactions, diamines of various lengths were complexed to acidic amino acids, aspartic and glutamic acids and crystallized. The following structures were determined by single-crystal X-ray diffraction studies. Putrescine complexed with:

1. L–glutamic acid
2. DL–glutamic acid
3. L–aspartic acid

Propanediamine complexed with:

4. L–glutamic acid
5. DL–glutamic acid

Hexanediamine complexed with:

6. L–glutamic acid.

4. Polyamine binding to viral genomes

It has been known that certain plant viral genomes bind specific polyamines while others do not. It is possible that the information for polyamine binding is contained in the genomic sequences of these viruses. A systematic analysis of the polyamine binding and non-binding viral genomic sequences was therefore carried out.

5. Crystallization of polyamine salts and complexes

Crystallization is the first step towards successful determination of structure by X-ray diffraction. Sym-homospermidine was purified from sandal leaves following published procedures and its phosphate salt crystallized by liquid diffusion of propanol. Free polyamines were prepared from commercially available chloride salts by ion-exchange chromatography. The free amine was titrated with aspartic or glutamic acid till the pH reduced to 7. This was concentrated by lyophilization. The aqueous concentrate was layered with a variety of non-polar solvents and left standing to undergo liquid diffusion. Though many solvents were tried, crystals useful for diffraction studies were usually obtained with propanol.

6. Structures of polyamine salts

The crystal structure determination of the chloride salt cadaverine completes the structural investigation on diamine chloride salts and also provides information on this unusually difficult structure. Sym-homospermidine is a naturally occurring analog of spermidine. The phosphate group in the structure presented here is in its mono-ionic form unlike the di-ionic form present in the structure of spermidine phosphate. Both the amines have an all *trans* conformation in their structures. There are two cadaverine molecules in the asymmetric unit. The arrangement of the bent cadaverine molecules in the unit cell is such that there exists a water channel with a disordered water molecule between the concave surfaces of the amine, while the space between the convex surfaces is not large enough to accommodate water molecules.

7. Structures of complexes

Packing in the crystals of the putrescine complexes are similar to the amine sandwiched between two

amino acids. This type of packing allows the amines to have van der Waals type of interactions with the backbone nonpolar atoms of the amino acids. In order to achieve this, the putrescine assumes a *gauche-trans-gauche* conformation in the aspartic acid complex. In the other two complexes the putrescine is present with an all *trans* conformation. The packing of molecules in the complexes of propanediamine with L and DL glutamic acids is very different. In the DL–complex it is similar to the packing in the putrescine complexes with the amine sandwiched between two glutamic acid molecules of the same chirality, suggesting this could be the structure in solution as well as in its L-complex. However, the basic packing unit in the propanediamine L–glutamic acid structure are dimers of glutamic acid molecules interspersed with propanediamines. The propanediamine, in order to effectively pack in such a situation, assumes a *trans-gauche* conformation. The hexanediamine glutamic acid complex is the only complex in which there are water molecules of crystallization. The distance between the carboxyl groups of glutamic acid, irrespective of the conformation of the glutamic acid molecule, is shorter than the distance between the amino groups of hexanediamine in its all *trans* conformation. Water molecules act as hydrogen bonding bridges between the amino groups of hexanediamine and the carboxyl groups of the amino acid.

8. Analysis of interactions

The major aim of determining these structures was to perform a systematic analysis of the electrostatic, hydrogen bonding and van der Waals interactions in these structures and understanding their implication for the binding properties of polyamines. Procedures for these analyses were developed and applied to the complexes. The stability of these complexes depends on the contributions from all the three types of interactions. The relative strengths of these interactions in three of these complexes were quantitated. The capacity of polyamines to take part in all the three types of interactions is probably one of the reasons for their choice as biological cations.

9. Analysis of viral genomic sequences

Polyamines bind selectively to certain plant viruses. In an attempt to explain this selectivity, sequences of 30 plant viral genomes from the EMBL database were chosen and analysed. No consensus sequence was found in polyamine binding viruses that could be attributed to sites of binding. However, it was noticed that the departure from expected frequencies of dinucleotides was greater in polyamine-binding viruses. A skewness parameter, defined to signify the deviation from the anticipated frequency, was computed. Polyamine-binding viruses had the largest skewness parameters. Also the change in frequency from anticipated values of complementary oligonucleotides was simultaneously higher or lower in these viruses. Computations were performed to understand this phenomena. These computations establish a definite correlation between polyamine binding and double helical potential in excess of the extent anticipated for random distribution of nucleotides. This property along with the presence or absence of the basic amino terminal arm might be determinants of polyamine binding.

Most of the results are published in the references listed[1–9].

References

1. RAMASWAMY, S., NETHAJI, M. AND MURTHY, M. R. N. — Crystal structure of putrescine–glutamic acid complex, *Curr. Sci.*, 1989, **58**, 1160–1162.
2. RAMASWAMY, S. AND MURTHY, M. R. N. — Crystal structure of putrescine–aspartic acid complex, *Curr. Sci.*, 1990, **59**, 379–382.
3. RAMASWAMY, S. AND MURTHY, M. R. N. — Crystal structure of hexanediamine–glutamic acid complex, *Curr. Sci.*, 1991, **60**, 173–176.
4. RAMASWAMY, S. AND MURTHY, M. R. N. — Crystal and molecular structure of putrescine DL-glutamic acid complex, *Curr. Sci.*, 1991, **61**, 410–413
5. RAMASWAMY, S. AND MURTHY, M. R. N. — Crystal and molecular structure of sym-homospermidine monohydrate, *Indian J. Biophys. Biochem.*, 1991, **28**, 504–512.
6. RAMASWAMY, S. AND MURTHY, M. R. N. — Crystal structures of propanediamine complexed with L and DL-glutamic acid: effect of chirality on propanediamine, *Acta Crystallogr. B*, 1992, **48**, 488–492.

7. RAMASWAMY, S. AND MURTHY, M R N. Crystal structure of cadaverine dihydrochloride monohydrate, *Indian J Biochem Biophys.*, 1992, **29**, 402–406

8. RAMASWAMY, S AND MURTHY, M R N. Polyamines. structure and interactions (communicated to *Biopolymers*)

Thesis Abstract (Ph.D.)

Conformational studies on globular proteins: data analysis by N. Srinivasan.
Research supervisor: C. Ramakrishnan.
Department: Molecular Biophysics Unit.

1. Introduction

Identification and understanding of general features present in three-dimensional structures of proteins is a useful and active area of research[1] This provides information on similar features in dissimilar proteins and hence reflects on characteristics of proteins in general[2-5]. Extraction and analysis of features in unrelated protein structures available in protein data bank (PDB)[6] are ideally suited for this purpose[7].

2. Materials and method

For most part of the study a data set containing 65 protein structures which are predominantly non-homologous and whose crystal structures are available at resolution 2 Å or better is used. This data set contains proteins from diverse families performing different functions. Many sub-databases were created from the original coordinate data. These include sub-database on amino acid sequence, the (ϕ, ψ) values, C^{α} positions, secondary structure assignments using (ϕ, ψ) values and surface residues. These databases have been extensively used in extraction of information and analysis of features in proteins.

3. Results

3.1. *The (ϕ, ψ) distribution of amino acid residues in proteins*

The contact map arrived at by Ramachandran and coworkers[8,9] has a profound influence in the understanding of protein conformation. The Ramachandran map shows the stereochemically allowed and disallowed (ϕ, ψ) space. Although considerable amount of (ϕ, ψ) space is allowed it is possible that individual amino acid residues in proteins would favour or disfavour certain local conformational regions within the allowed space. The (ϕ, ψ) plot of each of the 20 amino acid residues in proteins was studied. Conformational preference or otherwise was studied in 60° grids in the (ϕ, ψ) plane as well as in five regions defined in the allowed space. This was performed using non-Gly, non-Pro distribution as a reference (Fig. 1). The entire allowed regions of (ϕ, ψ) were partitioned into five regions corresponding respectively to: (i) extended conformation regions with positive ψ, (ii) bridge region, (iii) α_R region, (iv) extended region with negative ψ, and (v) α_L region. The propensity values of 20 amino acid residues in these regions are given in Table I. Some of the interesting results are as follows:

(1) Asn is the most prominent non-glycyl residue to occur in the partially allowed regions of the Ramachandran map, particularly in α_L region.

(2) Gly has the maximum disfavour to occur in the extended region.

(3) Ile and Trp conformations seldom occur in the α_L region and Thr conformations occur very rarely in this region; and

(4) Polar residues take up conformations in partially allowed regions more frequently than non-polar residues.

3.2. *Conformational aspects of glycyl residue*

Glycyl residues occupy a special and unique status as they can enjoy more conformational freedom than

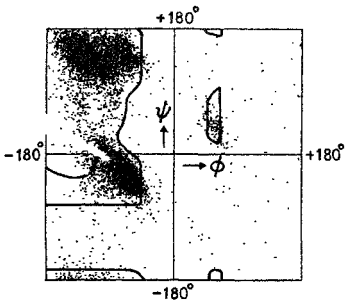

(a)

+180°

	14·3	19·8	1·9	0·1	0·1	0·1
	3·1	6·1	0·3	0·2	0·1	0·1
	1·1	3·7	0·1	1·1	0·9	
−180°	0·7	33·1	9·8		0·2		+180°
	0·1	0·5	0·7	0·1		
	0·7	0·6		0·1	0·1	0·1

−180°

(b)

FIG. 1. Distribution of conformational points of non-Gly, non-Pro residues in the present data set.
(a) The (ϕ, ψ) plot, superimposed on the Ramachandran map, (b) The grid plot showing the percentage distribution of points in 60° × 60° grids. Only non-zero percentages are shown.

Table I
Propensity of occurrence of conformations of various residues at five regions in the (ϕ, ψ) plane

Residue	*Propensity values at conformational regions I to V*				
	I	*II*	*III*	*IV*	*V*
Ala	0·79	0·96	1·23	0·46	0·65
Arg	0·94	0·73	1·15	0·38	0·70
Asn	0·77	2·50	0·75	3·08	6·17
Asp	0·80	1·83	1·03	2·15	1·52
Cys	1·29	0·54	0·76	1·46	0·78
Gln	0·89	0·73	1·12	0·85	1·26
Glu	0·68	0·79	1·39	0·00	0·52
Gly	0·31	0·60	0·36	5·85	9·48*
His	1·01	1·58	0·87	1·08	1·61
Ile	1·27	0·44	0·90	0·46	0·00
Leu	1·02	0·69	1·10	0·15	0·35
Lys	0·84	0·75	1·17	0·85	1·22
Met	1·04	0·65	1·04	0·00	0·65
Phe	1·07	1·15	0·97	0·77	0·83
Pro	0·92	0·50	0·91	1·08	0·00
Ser	1·05	1·29	0·88	1·54	0·74
Thr	1·14	1·04	0·83	2·85	0·00
Trp	1·06	1·27	0·99	0·92	0·00
Tyr	1·25	1·00	0·75	0·38	1·22
Val	1·35	0·40	0·83	0·31	0·17

* 14·74 if one considers the bridge region on the right side of the glycyl steric map.

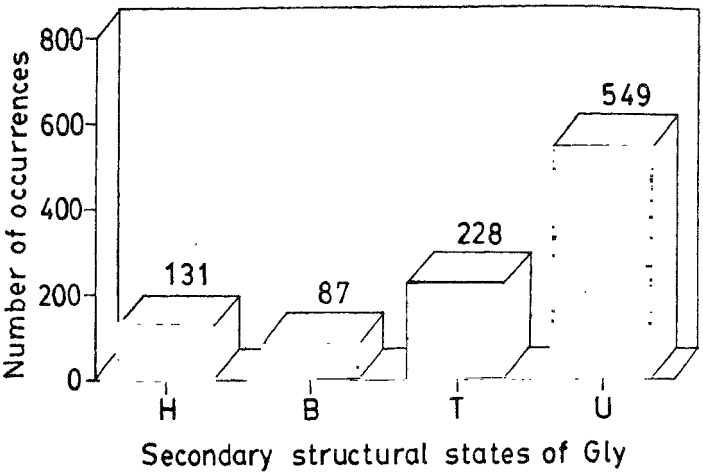

FIG. 2. Bar diagram showing the distribution of glycyl residues in the present data set, in the four secondary structural states. H (Helix), B (extended strands), T (turns) and U (uncharacterized segments).

any other residue. The occurrence of glycyl residues at primary, secondary and tertiary structure levels of proteins was investigated. The glycyl conformations in peptides were analyzed for (ϕ, ψ) preferences and compared with those in proteins. The occurrence of glycyl residues in different secondary structures was also analyzed (Fig. 2). All these studies resulted in the identification of several interesting features. Some of these are:

(1) The (ϕ, ψ) plot of Gly tend to cluster also around ($-90°$, $0°$) in peptides and near right-handed α-helical region in proteins.
(2) Gly is known to have poor potential for helices. But in helix-rich proteins it has a higher preference to occur in helices.
(3) The conformational freedom of Gly is effectively used to prefer those positions in turns that are less favourable for non-Gly residues; and
(4) Only one third of all the Gly are situated at surfaces.

Although the Ramachandran map for glycyl residue is symmetric in nature, it is possible that glycyl conformations in proteins can have preference to occur in the left or right half of the (ϕ, ψ) plane. A survey of nearly 1200 glycyl residues in proteins resulted in several doublets and triplets where the glycyl conformations show definite preference to occur in the left or right half of the (ϕ, ψ) plane.

By computing confidence coefficient for the various X-Gly-Y triplets, it has been possible to find out bias, if any, of the glycyl residue sandwiched between two specific residues X and Y to adopt conformation in the right or left half of the (ϕ, ψ) plane. A list of X-Gly-Y triplets was arrived at, where Gly prefers to adopt positive ϕ value (P-predominant) (Table II). Similarly, some other X-Gly-Y sequences have preference for negative ϕ values at Gly (N-predominant) (Table II).

Attempts were made to find out a possible reason for preference for positive ϕ value at Gly in P-predominant triplets. A prominent triplet, Asp-Gly-Lys which is P-predominant is chosen for a case study. Detailed stereochemical investigations on an example of Asp-Gly-Lys present in conconavalin A

Table II

The P and N predominant X-Gly-Y triplets

(a) P-predominant triplets

X-Gly-Y	*No. of examples in P and N regions (p:n)*	*Confidence coefficient (P_p)*
Asp-Gly-Lys	8:0	0·9961
Asn-Gly-Ser	6:0	0·9844
Pro-Gly-Thr	6:0	0·9844
Asn-Gly-Gly	5:0	0·9688
Asp-Gly-Asn	5:0	0·9688
Ser-Gly-Thr	8.2	0·9453
Val-Gly-Ala	6:1	0·9375
Gln-Gly-Asp	4:0	0·9375
Gln-Gly-Gly	4:0	0·9375
Glu-Gly-Asn	4:0	0·9375
Ser-Gly-Asn	4:0	0·9375
Ser-Gly-Glu	4:0	0·9375
Ala-Gly-Gly	7:2	0·9102
Asp-Gly-Ser	7·2	0·9102
Ser-Gly-Ala	7:2	0·9102
Cys-Gly-Lys	3:0	0·8750
Glu-Gly-Tyr	3:0	0·8750
Lys-Gly-Leu	3:0	0·8750
Pro-Gly-Gln	3:0	0·8750
Val-Gly-Gly	10:5	0·8491
Asp-Gly-Val	4:1	0·8125
Ile-Gly-Arg	4:1	0·8125
Leu-Gly-Ile	4:1	0·8125
Thr-Gly-Leu	4:1	0·8125
Ala-Gly-Ala	8:4	0·8062

(b) N-predominant triplets

X-Gly-Y	*No. of examples in P and N regions (p:n)*	*Confidence coefficient (R_n)*
Leu-Gly-Phe	0:6	0·9844
Pro-Gly-Val	0:6	0·9844
Cys-Gly-Gly	1:7	0·9648
Ile-Gly-Ile	0:4	0·9375
Ala-Gly-Val	2:7	0·9102
Gly-Gly-Pro	2.7	0·9102
Ala-Gly-His	1:5	0·8906
Gly-Gly-Gly	1:5	0·8906
Val-Gly-Lys	1:5	0·8906
Asn-Gly-Glu	0:3	0·8750
Asn-Gly-Pro	0:3	0·8750
Asp-Gly-Glu	0:3	0·8750
Trp-Gly-Leu	0:3	0·8750
Val-Gly-Arg	0:3	0·8750
Val-Gly-Ile	0:3	0·8750
Leu-Gly-Gly	3:7	0·8281
Gly-Gly-Cys	1:4	0·8125
Ile-Gly-Val	1:4	0·8125
Leu-Gly-Val	1:4	0·8125

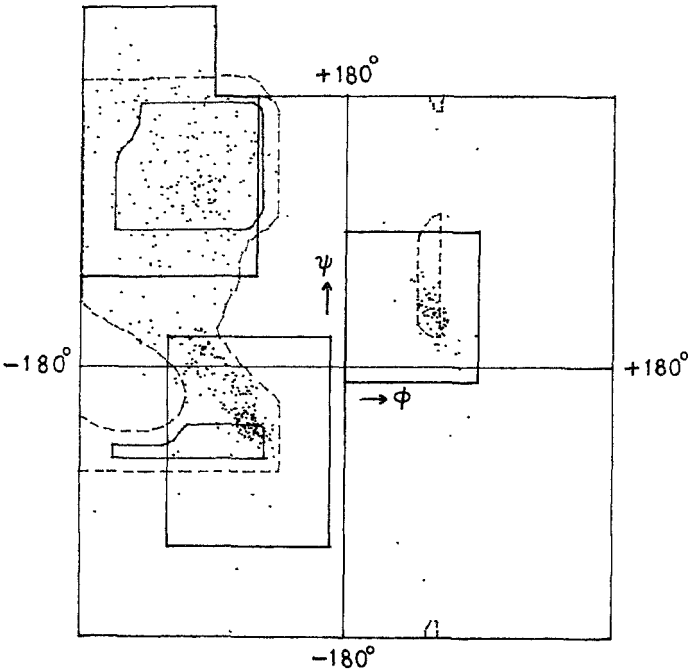

FIG. 3. The (ϕ, ψ) plot of Asn residues in proteins, superimposed on the Ramachandran map The extended conformation in the left bottom quadrant are plotted above the left top quadrant to emphasize clustering around the β-region. Conformation clusterings are highlighted by means of rectangles.

was carried out. Stepwise introduction of atoms at the X position of X-Gly-Y indicates that side chain of Asp which is preceding Gly restricts the range of ϕ at Gly and confines it to the positive values. This is true only if ψ at Gly is close to 0° and this becomes a natural outcome as there is a good concentration of Gly residues around $\psi = 0°$.

3.3. *Conformation of Asn residues*

Among the non-Gly residues, Asn is the prominent resudue to adopt α_L conformation. Conformations of about 500 Asn residues in 65 proteins have been analyzed for preferences in the specified local regions of the Ramachandran map. Three local regions are chosen and they are (1) α_L, (2) α_R and (3) extended (Fig. 3).

Many of the Asn residues with α_L conformation are present in β-turns. Quite a few interesting features concerning the positional and conformational preference of Asn residues in the four positions of various β-turn types are identified. A conclusion based on observations concerning Asn in i and $i + 3$ positions of β-turns

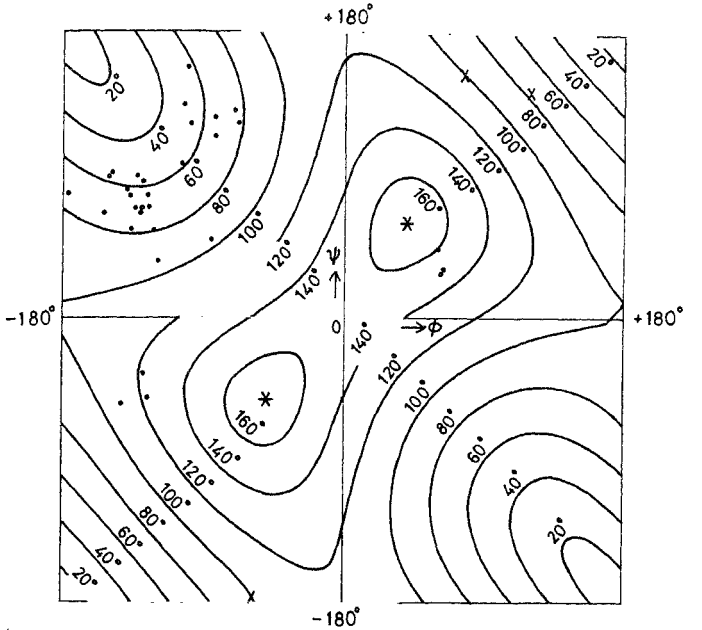

FIG 4. Variation of angle between the helices as a function of (ϕ, ψ) at the linker in the model $\alpha\alpha$ motif. (ϕ, ψ) values of observed single-residue $\alpha\alpha$ linkers are also plotted. X–Glycyl conformations; *–160° contours.

is that consistent features having better ordering than a simple β-turn do exist in proteins. Preference of Asn residues to occur in various locations (ends or middle) of helices and extended strands are also identified.

3.4. *Helix–linker–helix motifs in proteins*

It is well established that α_L conformations occur in certain types of β-turns or more generally in segments which link regular secondary structures. A class of such motif, namely, helix–linker–helix was taken up for a detailed study.

The stereochemistry and topology of a model helix–linker–helix system are analyzed. The system consists of two $(Ala)_9$ segments in right-handed α-helical structure hinged at an α-carbon atom so that the variation of (ϕ, ψ) values at the hinge brings about either a change of direction of second helix with respect to the first one or just displaces it. The allowed (ϕ, ψ) values at the linker (hinge) are arrived at using the well-known contact criteria[8]. An interesting outcome of the steric map is that the extended conformations at the linker are not stereochemically allowed. The angle between the helices for various pairs of (ϕ, ψ) values at the linker

are worked out and it is represented as a contour plot in Fig. 4. A striking feature is that if the linker adopts α_L conformation the structure is overall straight with one helix getting displaced with respect to the other and propagates without change in the direction. The deduction based on this model system is compared with examples in observed protein structures and the agreement is generally good.

102 examples of helix–linker–helix extracted from 65 proteins were analysed. Only those $\alpha\alpha$ motifs where the linker contains 5 residues or less are considered for analysis. The distribution of angle between the helices and end-to-end distance of linkers was studied for consolidated data as well as for each of the 1 to 5 residue linkers. Amino acid residue preferences at the linkers, last location of the preceding helix and the first location of the succeeding helix were also analyzed. The amino acid residues, Gly, Asp, Pro, Ser and Thr are prominent in linkers and Pro is also prominent in the first position of the succeeding helix. The conformational preferences at various residues in the linkers as well as the conformational families are identified. A prominent conformational family corresponds to three residues in the linker adopting $\alpha_L\beta\beta$ conformation where α_L conformation is invariably taken up by Gly.

4. Outlook

The work carried out has thus resulted in many new observations and strengthening of some known ideas. Thus, it contributes towards our understanding of protein structures and the results can be expected to be very useful in prediction, modelling, design and engineering of protein structures.

References

1. RICHARDSON, J. S. AND RICHARDSON, D. C. — In *Prediction of protein structure and principles of protein conformation*, (G. D. Fasman, ed), 1989, pp 1–98, Plenum Press.
2. ARGOS, P — *J Mol. Biol.*, 1987, **197**, 331–348
3. WILMOT, C. M AND THORNTON, J. M. — *J. Mol Biol* , 1988, **203**, 221–232.
4. EFIMOV, A. V — *Protein Engng*, 1991, **4**, 245–250.
5. SRINIVASAN, N., SOWDHAMINI, R., RAMAKRISHNAN, C. AND BALARAM, P — In *Molecular conformation and biological interactions* (P. Balaram and S. Ramaseshan, eds) 1991, pp 59–73, Indian Academy of Sciences, Bangalore.
6. BERNSTEIN, F. C., KOETZLE, T. F. WILLIAMS, G. J. R., MEYER, E. F. Jr, BRICE, M. D., RODGERS, J. R., KENNARD, O., SHIMANOUCHI, T. AND TASUMI, M. — *J Mol. Biol.*, 1977, **112**, 535–542.
7 THORNTON, J M. AND GARDNER, S. P. — *Trends Biochem Sci.*, 1989, **14**, 300–304.
8. RAMACHANDRAN, G. N., RAMAKRISHNAN, C. AND SASISEKHARAN, V — *J. Mol. Biol.*, 1963, **7**, 95–99.
9. RAMACHANDRAN, G. N. AND SASISEKHARAN, V — *Adv. Protein Chem.*, 1968, **23**, 283–437.

Thesis Abstract (Ph.D.)

Structural studies on peanut lectin by Shekhar C. Mande.
Research supervisor: M. Vijayan.
Department: Molecular Biophysics Unit.

1. Introduction

Lectins form a diverse group of carbohydrate-binding proteins of non-immune origin and are characterized by their ability to agglutinate cells. Although first discovered in plant seeds, lectins have also been detected and purified from several other sources. Among plants, Legumonicae is by far the richest underexplored family of proteins in terms of structure–function relationships. The only legume lectins whose three-

dimensional structures were available until recently were concanavalin A (con A)[1,2], pea lectin[3] and favin[4]. Crystallographic studies on peanut lectin were initiated in this laboratory with the ultimate objective of determining its polypeptide conformation and correlating the structure with function. Peanut lectin exhibits specificity for the T-antigen, D-Gal β1-3 D-GalNac. At physiological pH, it exists as a tetramer, molecular weight 110,000, consisting of four identical polypeptide chains.

2. Crystallization, preliminary studies and high-resolution data collection

The protein was crystallized earlier in one orthorhombic, two monoclinic and one triclinic crystal forms[5,6]. The crystals belonging to the orthorhombic space group $P2_12_12$ with unit cell dimensions $a=129.3$, $b=126.9$, $c=76.9$ Å appeared to be the most suitable for carrying out further analysis. Intensity data on these crystals were collected initially at low resolution. Self-rotation functions calculated using these data and chemical crosslinking experiments carried out in parallel, suggested the protein to be a dimer of a dimer with 222 symmetry[7]. High-resolution (2.4 Å) intensity data were collected using oscillation photography followed by computer-controlled microdensitometry. To collect the entire data, 36 crystals and 67 film packs were used. A total of 40899 unique reflections were derived from 153631 reflections recorded, with a merging R-value of 0.114. Self-rotation functions calculated using the high-resolution data reinforced the conclusions regarding the quaternary structure of peanut lectin.

3. Structure solution

Following reports that legume lectins exhibit circularly permuted sequence homology among themselves[8], the available partial sequence of peanut lectin[9] was compared with those of con A, pea lectin and favin[10]. A detailed comparison led to the conclusion that peanut lectin has a reasonable degree of overall sequence homology with the other three lectins. The metal-binding sites in all the four lectins are conserved. Also, substantially conserved are glycines with conformation appropriate for D-amino acids. The carbohydrate-binding regions show considerable variability.

In view of the above, it appeared reasonable to approach the structure solution through the molecular replacement method. Initial calculations were carried out using con A tetramer and dimer and pea lectin dimer as models. Each of the rotation functions calculated using these models indicated two distinct solutions. The solution to the translation problem was attempted by packing hard spheres of different radii in the unit cell, and later through R-factor and correlation coefficient searches. Several R-factor and correlation coefficient searches with con A model oriented in the neighbourhood of the two possible solutions obtained from the rotation functions failed to yield a solution to the translation problem.

Twenty-two plausible tetrameric, dimeric and monomeric search models were then constructed after a careful examination of the two sets of con A coordinates in the protein data bank and pea lectin coordinates. In many of the search models, only the regions common to con A and pea lectin were chosen. Cross-rotation functions using these models confirmed two possible solutions to the rotation problem identified earlier. The region of the asymmetric unit to be searched for the solution of the translation problem was demarcated by packing analysis using a novel program developed by the author[11]. Subsequent exhaustive R-factor and correlation coefficient searches using two plausible tetrameric models again failed to yield the position of the molecule in the cell. The possibility of a solution with the molecule located on crystallographic two-fold axes was also carefully explored, but in vain.

While the rotation and translation searches outlined above were being pursued, attempts were also underway for preparing isomorphous heavy atom derivatives. Data from six derivatives up to resolutions varying between 3.8 and 3.2 Å and fresh native data up to a resolution of Å were collected. The heavy atom positions were determined and later refined using well-known crystallographic techniques. The occupancies of heavy atom constellations in the three platinum derivatives, two involving K_2PtCl_6 and one involving K_2PtCl_4 were related to one another and had no symmetry among the sites. The other three derivatives involving samarium nitrate, iodophenyl galactose and gold chloride had four heavy atom sites each; in each case, the sites were related to one another by approximate 222 symmetry. The results of the phase angle calculations indicated phasing to be good at low angles but poor at high angles. Therefore,

an electron density map was calculated at 5.5 Å resolution. The tetrameric molecule could be clearly distinguished from the solvent regions in the map. The centre of the density corresponding to the molecule occurred at a position found to be allowed in the earlier packing analysis. The low-resolution map unambiguously establishes the gross structure of peanut lectin, which is entirely consistent with different rotation functions and packing analysis, and sets the stage for a future high-resolution analysis in terms of the polypeptide chain conformation.

References

1. HARDMAN, K. D. AND AINSWORTH, C. F. — *Biochemistry*, 1972, **11**, 4910–4919.
2. REEKE, G. N., BECKER, J. W. AND EDELMAN, G. M. — *J. Biol. Chem.*, 1975, **250**, 1525–1547
3. EINSPAHR, H., PARKS, E. H., SUGUNA, K., SUBRAMANIAN, E. AND SUDDATH, F. L. — *J. Biol. Chem.*, 1986, **261**, 16518–16527.
4. REEKE, G. N. AND BECKER, J. W. — *Science*, 1986, **234**, 1108–1111.
5. SALUNKE, D. M., KHAN, M. I., SUROLIA, A. AND VIJAYAN, M. — *J. Mol. Biol.*, 1982, **154**, 177–178.
6. SALUNKE, D. M., KHAN, M. I., SUROLIA, A. AND VIJAYAN, M. — *FEBS Lett.*, 1983, **156**, 127–129.
7. SALUNKE, D. M., SWAMY, M. J., KHAN, M. I., MANDE, S. C., SUROLIA, A. AND VIJAYAN, M. — *J. Biol. Chem*, 1985, **260**, 13576–13579.
8. HEMPERLEY, J. J. AND CUNNINGHAM, B. A. — *TIBS*, 1983, 100–102.
9. LAUWEREYS, M., FORIERS, A., SHARON, N. AND STROSBERG, A. D. — *FEBS Lett.*, 1985, **181**, 241–244.
10. MANDE, S. C., RAGHUNATHAN, S., SALUNKE, D. M., KHAN, M. I., SWAMY, M. J., SUROLIA, A. AND VIJAYAN, M. — *Indian J. Biochem. Biophys.*, 1988, **25**, 166–171
11. MANDE, S. C. AND SUGUNA, K. — *J. Appl. Crystallogr.*, 1989, **22**, 627–629.

Thesis Abstract (Ph.D.)

Immunochemical studies on serum retinol binding proteins and beta-lactoglobulin by B.M.M.M. Kumar Reddy.
Research supervisor: P. R. Adiga.
Department: Biochemistry.

1. Introduction

Retinol-binding protein (RBP) transports Vitamin A in plasma. RBP has retained its physicochemical and functional characteristics during the vertebrate evolution. Surprisingly a measurable degree of immunological crossreactivity among various RBPs is largely confined to a given mammalian order and little occurs outside it. In addition, RBP represents a new family of proteins, whose function is to bind and transport various hydrophobic molecules. This family includes β-lactoglobulin (BLG) and placental protein-14 (pp-14). Both these proteins share a functional as well as structural homology with RBP. In the present work, attempts have been made to study and compare the immunotopography of these proteins using monoclonal antibodies (MAbs).

2. Experimental procedures

RBP was purified from the pooled plasma by ion-exchange chromatography, preparative polyacrylamide gel electrophoresis and gel filtration chromatography. Monoclonal antibodies (MAbs) were raised against chicken, human RBPs and BLG using the hybridoma technology. MAbs were characterized by their subclass isotyping. Crossreactivity among various RBPs was demonstrated by solid and liquid phase radioimmunoassays. RBP was chemically cleaved at methionine residues by cyanogen bromide and the peptides were purified and characterized by N-terminal sequencing. Various hydrophilic peptides were synthesized on polyethylene pins using F-moc chemistry and checked for MAb binding using ELISA technique

3. Results and discussion

Retinol-binding protein (M_r 21,000) is obligatory for retinol transport. RBP circulates in the plasma bound to thyroxine-binding prealbumin (transthyretin) in a 1:1 stoichiometry. During the evolution of the species, RBP has retained its physicochemical and functional characteristics including its primary structure. Thus, out of 182 amino acids available for comparison, over 150 are highly conserved. However, in radioimmunoassays utilizing polyclonal antibodies to either chicken, human or rat RBPs no gross immunological crossreactivity was encountered among the RBPs from different mammalian species. With a view to understand the immunotopography of these proteins, it was decided to raise MAbs against chicken as well as human RBPs.

Four groups of MAbs (F4C4, D9D2, C5E11 and H5D11) were raised against chicken RBP. MAb F4C4 recognized only chicken RBP whereas MAb C5E11 recognized all the RBPs tested. The other two MAbs exhibited similar characteristics in terms of binding to chicken, monkey and human RBPs. All the MAbs, except C5E11 recognized the circulatory RBP+transthyretin complex. MAb C5E11 failed to recognize the native as well as the circulatory RBPs and partial denaturation of RBP was essential for its binding. Since the primary structure of human RBP is known, further work was carried out with human RBP and anti-human RBP MAbs.

Four groups of MAbs recognizing distinct epitopes were raised against human RBP. These were termed B10E3, C1C5, F5C6 and G4E4. All the MAbs except G4E4 failed to recognize chicken RBP. In order to identify the sequences recognized by various MAbs, RBP was subjected to cyanogen bromide cleavage and a C-terminal peptide representing the residues 74–182 was isolated and characterized. MAbs C1C5 and G4E4 exhibited a significant binding to this peptide thereby showing the location of their respective epitopes in the C-terminal region of the molecule. The exact epitopic sequences recognized by MAb C1C5 was further elucidated using the synthetic peptides and found to be TCAD (residues 128–131). However, the minimal epitopic sequence required for MAb G4E4 could not be identified using the synthetic peptides. The failure to decipher its epitopic location by synthetic peptide approach may then be ascribable to the limited capacity of short synthetic peptides assuming appropriate conformation under the experimental conditions employed. The negative results obtained, using the C-terminal peptide, for MAbs F5C6 and B10E3 suggested the possible location of their respective epitopes in the N-terminal region of the protein; in fact, it was found that the epitopic sequence (FSVDE, residues 45–49) for MAb F5C6 was located in the N-terminal region (FSVDE, residues 45–49). MAb B10E3 recognized the discontinuous epitope and therefore its exact location could not be identified. In addition, the capacity of these MAbs to recognize the native, denatured and transthyretin-bound RBPs was extensively studied.

The recently elucidated structural homologies among BLG, RBP, Apolipoprotein D, HC protein and BG protein from olfactory epithelium have enabled their classification as members of a new protein superfamily of hydrophobic molecule transporters. RBP and BLG exhibit a remarkable structural and functional similarity. The polyclonal antibodies raised against BLG recognized RBP in a dose-dependent manner thereby showing the presence of similar epitopes on these two proteins. Therefore, it was worthwhile to raise MAbs to BLG and identify the common and distinct epitopes shared by these proteins. Towards this, two groups of MAbs were raised against BLG. MAb H9E10 recognized BLG alone whereas MAb B7B10 recognized both BLG and RBP to a similar extent. In order to identify the exact sequences responsible for MAb B7B10 binding, its reactivity was tested with the CNBr fragment (residue 74–182) of human RBP. The MAb exhibited a strong binding to this peptide and the sequence comparison of this

CNBr peptide and BLG revealed a linear structure of common sequence DTDY (residues 108-111 in human RBP and residues 96–99 of BLG). To delineate the exact amino acid sequence recognized by this MAb, a series of peptides containing DTDY at its core and flanked by others as present both in BLG and RBP were synthesized and the propensity of these peptides to bind the MAb was investigated. MAb B7B10, in fact, recognized all the DTDY-containing sequences and not the others.

It is intriguing that though polyclonal antibodies raised to BLG could recognize hRBP, the reverse was not observed. Similarly, none of the several MAbs raised to chicken RBP or human RBP recognized BLG. On the other hand, at least three clones were obtained from BLG-immunized mice, which were similar to B7B10 in terms of their capacity to recognize human RBP. These observations may be indicative of subtle differences between BLG and RBP in terms of elicitation of immune response to the DTDY-bearing sequence.

Placental protein PP-14 secreted by human endometrium exhibits a significant sequence homology (53·4%) with BLG and contains DTDY (residues 96–99) sequence in its primary structure. MAb B7B10 crossreacted with PP-14 in the tissue sections of human endometrium.

These studies handsomely illustrate the potential of the MAb approach to probe the epitopes shared by proteins with as low as 25–30% sequence homology, despite the general belief that proteins having greater than 40% divergence in the amino acid sequence usually show no discernible immunological crossreactivity.

References

1. KUMAR REDDY, B. M. M. M., ANJALI A. KARANDE AND ADIGA, P. R — *Biochem. Int.*, 1990, **21**, 367–376

2. KUMAR REDDY, B. M. M. M., ANJALI A. KARANDE AND ADIGA, P. R — *Mol. Immunol.*, 1992, **29**, 511–516

Thesis Abstract (Ph.D.)

Crystal structure of low humidity monoclinic lysozyme at 1·75 Å resolution by Madhusudan.
Research supervisor: M. Vijayan.
Department: Molecular Biophysics Unit.

1. Introduction

Water plays a crucial role in the folding, structure and action of proteins. A dry protein is dead, or at best dormant, and it can regain its tertiary structure, mobility and function only through interaction with water. Protein crystals form an excellent system to study protein–water interactions, as about half their volume is made up of water. In this context, it has been shown earlier in this laboratory that many protein crystals, but not all, undergo reversible structural transformations, as evidenced by abrupt changes in unit cell dimensions, diffraction pattern and solvent content, when the environmental humidity is systematically varied[1, 2]. These water-mediated transformations have been shown to provide a useful tool for exploring the variability in protein hydration and its structural consequences. In addition to carrying out preliminary investigations on several protein crystals, the crystal structure of the low-humidity form of the well-known tetragonal hen egg-white lysozyme has been analysed earlier in this laboratory[3, 4]. A comparison of this structure with the already known native structure showed that the gentle removal of a small amount of bulk water, which is what water-mediated transformations involve, results in significant changes in the hydration shell although the hydration shell tends to move as a whole along with the protein molecule. These changes lead to structural perturbations in the protein, which are most pronounced in the regions

involved in substrate binding Encouraged by the results obtained on tetragonal lysozyme, the X-ray analysis of low-humidity monoclinic lysozyme was taken up. Indeed, monoclinic lysozyme exhibits the most remarkable water-mediated transformation observed so far. The two crystallographically independent molecules in the native crystals become equivalent in the low-humidity form which at 22% has the lowest solvent content among the protein crystals examined to date. The low-humidity monoclinic crystals diffract better than the native ones.

2. Experimental

Intensity data were collected, at a relative humidity of 88%, up to a resolution of 1·75 Å from low-humidity monoclinic lysozyme using oscillation photography followed by computer-controlled microdensitometry. The data were processed using programmes originally developed by Rossmann[5]. The final processed data set contained 8523 independent reflections.

Attempts to refine the structure using one or the other of the two crystallographically independent molecules in the native structure as the starting model did not succeed. Subsequently, the structure was solved using rotation function and R-factor calculations employing the molecule in low-humidity tetragonal lysozyme as the search model. The structure was refined using Hendrickson–Konnert-restrained least squares method[6], interspersed with model building based on Fourier maps. The final model, containing 997 protein atoms, 148 water molecules and 2 nitrate ions, and an R-factor of 0·175 for 7684 reflections with $F > 4\,\sigma(F)$ in the 10 to 1·75 Å resolution shell.

3. Discussion

The refined structure provides the most accurate description to date of the enzyme molecule. The protein molecules are densely packed in the crystal. Each molecule is surrounded by, and in contact with, 14 other such molecules. The interstices in this arrangement are filled with the solvent. It turns out that about 90% of the total solvent, mainly water, molecules in the structure could be located. They provide a wealth of information on protein–water interactions, favourable sites of hydration on the protein–water interactions, favourable sites of hydration on the protein surface, the hydration of secondary structural features and side chains, intermolecular solvent bridges and the water structure associated with proteins. A comparison of the low-humidity structure with the native structure shows that substantial rearrangement of molecules takes place during the transformation. Differences in detail also exist in the molecular structure of the protein.

A comparison of the protein molecule and its hydration shell with those in native tetragonal lysozyme[7], low-humidity tetragonal lysozyme[3], high-pressure tetragonal lysozyme[8] and triclinic lysozyme[9] leads to the delineation of the relatively rigid, moderately flexible and highly flexible regions of the molecule. The relatively rigid region forms a contiguous structural unit close to the molecular centroid and encompasses parts of the main β-structure and three α-helices. The hydration shell of the molecule contains 30 invariant water molecules. Many of them are involved in holding different parts of the molecule together or in stabilizing the local structure. Five of the six invariant molecules attached to the substrate binding region form part of a water cluster contiguous with the side chains of the catalytic residues 35 Glu and 52 Asp.

4. Conclusion

While pursuing the detailed study of low-humidity monoclinic lysozyme, the author has also been involved in the high-resolution X-ray analysis of the complexes of tetragonal lysozyme with two closely related indicator dyes bromophenol red (BPR) and bromophenol blue (BPB). The dyes BPR and BPB bind to lysozyme and inhibit its activity against bacterial cell wall, but not against the polysaccharide. The binding site of BPR had already been characterized earlier at 5·5 Å[10]. The 2 Å analysis of the BPR complex confirms this site to be outside the cleft close to subsite F. The 2 Å analysis of the BPB complex, however, shows that this dye binds close to subsites A and B. The pHs at which the dyes were soaked into the crystal were such that BPR (pH 4·6) was neutral and BPB (pH 5·6) was ionised. The results thus appear to indicate that the neutral and the ionised species of the dyes have different binding sites. These sites are perhaps involved in the interaction of the protein with the peptide component of peptidoglycan.

References

1. SALUNKE, D. M., VEERAPANDIAN, B AND VIJAYAN, M. — *Curr Sci*, 1984, **53**, 231–235.
2. SALUNKE, D M. VEERAPANDIAN, B, KODANDAPANI, R., AND VIJAYAN, M. — *Acta Crystallogr. B*, 1985, **41**, 431–435.
3. KODANDAPANI, R., SURESH, C. G. AND VIJAYAN, M. — *J. Biol Chem.*, 1990, **265**, 16126–16131.
4. VIJAYAN, M. AND KODANDAPANI, R — In *Molecular conformation and biological interactions* (P. Balaram and S. Ramaseshan, eds), 1991, Indian Academy of Sciences, Bangalore.
5. ROSSMANN, M G. — *Methods in Enzymology*, Vol 14, pp 237–280, 1985
6. HENDRICKSON, W. A. AND KONNERT, J. H. — In *Computng in crystallography* (R. Diamond, S. Ramaseshan and K. Venkatesham, eds), 1980, pp 13.01–13.26, Indian Academy of Sciences, Bangalore.
7. IMOTO, T., JOHNSON, L. N., NORTH, A. C. T., PHILLIPS, D. C. AND RUPLEY, J. A. — In *The enzymes* (P. D. Boyer, ed.), Vol. 7, 1972, pp 665–808, Academic
8. KUNDROT, J. H. AND RICHARDS, F M. — *J. Mol. Biol.*, 1987, **193**, 157–170.
9. RAMANADHAM, M., SIEKER, L. C. AND JENSEN, L. H. — *Acta Crystallogr. B*, 1990, **46**, 63–69.
10. VEERAPANDIAN, B., SALUNKE, D. M. AND VIJAYAN, M. — *FEBS Lett.*, 1985, **186**, 163–167.

Thesis Abstract (Ph.D.)

Stimulation of NADH oxidation and oxygen uptake by oxovanadium compounds by Kalyani Penta.
Research supervisor: T. Ramasarma.
Department: Biochemistry.

1. Introduction

The stimulation of NADH oxidation and of accompanying oxygen reduction by oxovanadium compounds has been studied in great detail[1]. The relevant chemistry of dioxygen (O_2), its activation and reduction to H_2O_2 and oxyradicals, the chemistry of the valence states of vanadium and their participation in the different redox reactions have been reviewed. The emerging information on hydrogen peroxide (H_2O_2) as a metabolically important molecule has been brought to focus[2–4]. Vanadate-dependent oxidation of NADH offers a model system for the rapid, transient generation of H_2O_2, occurring in variety of biological phenomena, *e.g.*, phagocytosis.

2. Materials and methods

Oxidation of NADH (100–200 μM) and accompanying oxygen uptake were monitored by visible spectroscopy and polarography. Meta-, deca- and polyvanadate were used at concentrations specified. Rat liver microsomes and plasma membranes were used as enzyme source. Free radicals generated were characterised using spin trapping and ESR spectroscopy. Vanadium solutions used were characterised by V^{51}NMR spectroscopy.

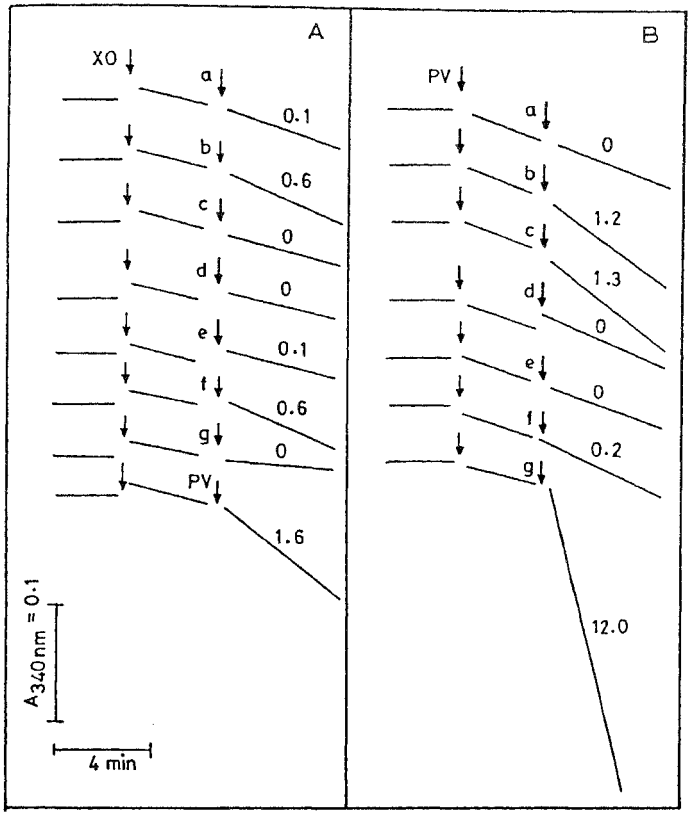

FIG. 1. Effect of addition of some purified dehydrogenases on NADH oxidation stimulated by xanthine oxidase and by polyvanadate. The reaction mixture contained 50 mM K-phosphate buffer (pH 7·0) and 100 μM NADH. Further additions were made of 43 μg xanthine oxidase (+ 100 μM xanthine) (XO) and 300 μM polyvanadate (PV) in the experiments A and B, respectively. After recording the initial rate of decrease in absorbance at 340 nm 100 μg each of dehydrogenases were added as marked: a. LDH (rabbit muscle), b. LDH (beef heart), c. malate dehydrogenase (pig heart), d. glutamate dehydrogenase (bovine heart), e. GAPD (rabbit muscle), f. GAPD (chicken liver), g. isocitrate dehydrogenase (pig heart). The numbers shown on the recordings are increases in rates of NADH oxidation as n moles/min due to addition of dehydrogenases (or PV). In experiments A where PV was added xanthine was omitted

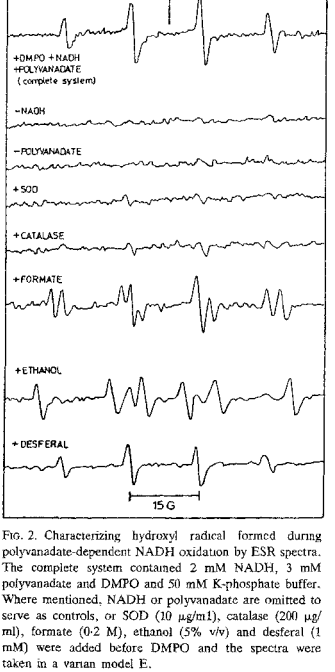

FIG. 2. Characterizing hydroxyl radical formed during polyvanadate-dependent NADH oxidation by ESR spectra. The complete system contained 2 mM NADH, 3 mM polyvanadate and DMPO and 50 mM K-phosphate buffer. Where mentioned, NADH or polyvanadate are omitted to serve as controls, or SOD (10 μg/ml), catalase (200 μg/ml), formate (0·2 M), ethanol (5% v/v) and desferal (1 mM) were added before DMPO and the spectra were taken in a varian model E.

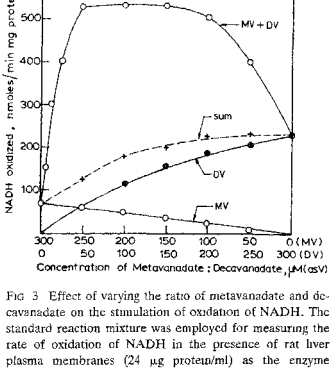

FIG 3 Effect of varying the ratio of metavanadate and decavanadate on the stimulation of oxidation of NADH. The standard reaction mixture was employed for measuring the rate of oxidation of NADH in the presence of rat liver plasma membranes (24 μg protein/ml) as the enzyme source The concentration of metavanadate decreased from right to left and that of decavanadate in the opposite direction. The ratio of MV·DV is shown on the top for each set of points The activity is expressed as n moles/min per mg protein. The additions are as follows o——o MV alone; ●——● DV alone; o——o MV+DV at the ratio shown; +---+ arithmetic sum of activities with MV and DV separately tested at the concentration in the mixture.

3. Results and conclusions

The rate of oxidation of NADH in the presence of xanthine oxidase increases to a small and variable extent on addition of high concentration of lactate dehydrogenase and some other dehydrogenases (Fig. 1). This heat insensitive activity is similar to polyvanadate stimulation with respect to pH profile and inhibition by superoxide dismutase (SOD). This polyvanadate-dependent activity occurs also in the presence of riboflavin, FAD, and FMN and the activity is further enhanced with a non-specific protein such as bovine serum albumin, suggesting that some flavoproteins may also possess this activity[5].

The rate of polyvanadate-stimulated oxidation can be enhanced several fold by the enzymes in rat liver microsomal or plasma membranes and both the oxidation of NADH and the uptake of oxygen are markedly inhibited by SOD. But the reduction of cytochrome c was not sensitive to inhibition even at high concentrations of SOD, and therefore does not represent superoxide formation. The reduction of cytochrome *c* by vanadyl sulphate (V^{IV}) also was not sensitive to inhibition by SOD. In presence of H_2O_2, all

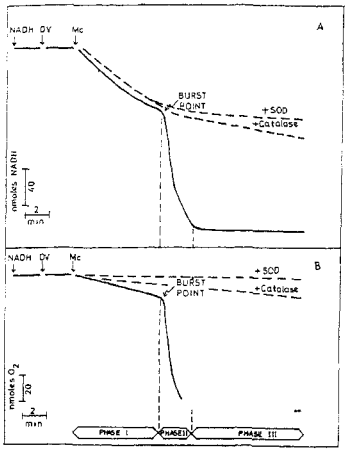

Fig 4. Decavanadate-dependent biphasic oxidation of NADH. The standard conditions of assay of oxidation of NADH (A) and of oxygen uptake (B) were used. Decavanadate (DV) was added at a concentration of 400 μM (as V). SOD (10 μg/ml) or catalase (100 μg/ml) were added before the addition of rat liver microsomes (Mc) and these reactions are marked by broken lines the initial slow oxidation, the rapid burst and the following release of oxygen are indicated as phases I, II, III, respectively

the forms of vanadate were able to oxidise reduced cytochrome *c*, which was sensitive to mannitol, tris and catalase, *indicating* H_2O_2-dependent generation of hydroxyl radicals. Using ESR and spin trapping technique, only hydroxyl radicals were detected during polyvanadate-dependent NADH oxidation[6] (Fig. 2).

Vanadate in the polymeric form, was found in our laboratory to be the most efficient in stimulating oxidation of NADH. Solutions obtained by extracting vanadium pentoxide with dilute alkali over a period of several hours, referred to as 'polyvanadate', contained increasing amounts of decavanadate ($V_{10}O_{28}^{6-}$). Using these solutions and a mixture of pure metavanadate and decavanadate, high activities of stimulation of NADH oxidation by rat liver plasma membranes were obtained when the ratio of metavanadate: decavanadate was in the range of 1–5, and decreased at higher and lower ratios (Fig. 3). The solutions used for these studies were characterised by NMR and IR spectroscopy. Increased activity was also obtained by reaching these ratios by conversion of decavanadate to metavanadate on alkaline degradation, and of metavanadate to decavanadate on acidification. These activities show for the first time that both deca and meta forms of vanadate, present in polyvanadate solutions, were needed for the maximal activity of oxidation of NADH[7].

The oxidation of NADH and the accompanying uptake of oxygen in the presence of decavanadate followed a novel biphasic pattern (Fig. 4). Phase I of this biphasic reaction involves reduction of decavanadate and generation of trace amounts of H_2O_2 on oxidation of NADH at a slow rate. The accompanying

rate of oxygen uptake in phase I is low and sensitive to inhibition by SOD. Catalase inhibits this oxygen uptake by 50%, whereas hydroxyl radical quenchers have no effect. On average three vanadium atoms were found to be reduced per V_{10} molecule. Phase II reaction is characterized by a rapid burst of oxidation of NADH and accompanying oxygen uptake. The properties studied suggest that it is a reaction dependent on reduced vanadium (V^{IV}) and H_2O_2. Phase II reaction is highly sensitive to SOD and catalase. The changes in visible spectra of the biphasic reaction confirm that V^{V} reduced during phase I is rapidly reoxidised during phase II. The stoichiometry of NADH:O_2 is 1:1 indicating H_2O_2 as the likely end product.

Vanadyl sulphate (V^{IV}), in the presence of trace amounts of H_2O_2, stimulates oxidation of NADH and oxygen and oxygen uptake without the addition of any enzyme. The stoichiometry of NADH:O_2 is 1:1 indicating H_2O_2 as the likely end product. Oxygen is rapidly consumed as in the burst during decavanadate-dependent reaction. The product of this oxidation of vanadyl is found to be a form of V^{V} compound by NMR analysis.

These studies showed that a mixture of meta and deca forms of vanadate gave maximum stimulation of NADH oxidation. Generation of OH but not of $O_2^{\cdot}$ radicals was detected in this recation with high rates of O_2 reduction to H_2O_2. Decavanadate showed initial slow rates, followed by a burst of oxidation of NADH and accompanying O_2 uptake similar to that obtained in the presence of trace amounts of H_2O_2.

References

1. RAMASARMA, T., VIJAYA, S., MEERA, R., LAKSHMI, K., PATOLE, M S., SHARADA, G., KALYANI, P., MIHIR, C. AND KURUP, C K. R — In *Biological oxidation systems* (C. Channa Reddy, G. A. Hamilton, and K M. Madhyastha, eds), Vol. 2, pp 909–928, 1990, Academic Press.
2. LAPORTE, F., DOUISSERRE, J AND VIGNAIS, P. — *Curr Top. Biochem.*, 1990, **194**, 301–308.
3. RAMASARMA, T. — *Biochem. Biophys. Acta*, 1979, **694**, 69–73.
4. MAY, J. M AND DE HAEN, C. — *J. Biol. Chem.*, 1979, **254**, 9017–9021
5. KALYANI, P., SHARADA, G., MEERA, R. AND RAMASARMA, T. — *Mol. Cell Biochem.*, 1991, **107**, 31–37.
6. KALYANI, P., VIJAYA, S. AND RAMASARMA, T. — *Mol. Cell. Biochem.*, 1992, **111**, 33–40.
7. KALYANI, P. AND RAMASARMA, T. — *Arch. Biochem. Biophys.*, 1992, **297**, 244–252.

Thesis Abstract (Ph.D.)

Inactivation of HMG CoA reductase by disfulfides, hydrogen peroxide, silatrane and ubiquinone by R. V. Omkumar.
Research supervisors: T. Ramasarma and C. K. R. Kurup.
Department: Biochemistry.

1. Introduction

The four-electron oxidoreductase 3-hydroxy-3-methylglutaryl coenzymeA reductase (HMG CoA reductase), being the rate-limiting enzyme in the biosynthesis of cholesterol in the liver, plays a key role in the regulation of serum cholesterol levels[1]. Understandably, knowledge of the physiological regulation of this enzyme, particularly by hypocholesterolemic agents and physiological modulators is of great medical relevance. The action of four such effectors on the enzyme (garlic disulfides, H_2O_2, 1-ethoxysilatrane and ubiquinone) is reported in this work.

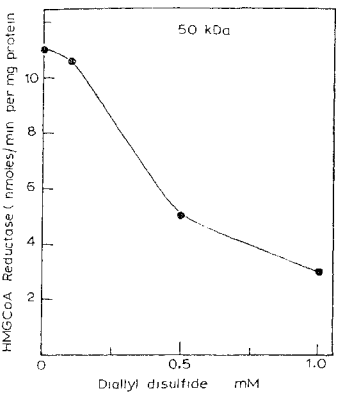

FIG. 1 Inhibition of soluble 50 kDa enzyme by diallyl-disulfide. Different concentrations of diallyldisulfide (in 1 μl alcohol) were preincubated with the soluble enzyme (0·019 mg) in phosphate buffer (100 mM, pH 7·4) for 20 min at 37°C. The reaction was started by adding DTT and the substrates

2. Materials and methods

The activity of HMG CoA reductase in rat hepatic microsomes and in membrane-free preparations was assayed by measuring the rate of formation of the product mevalonate (according to the reaction indicated below) using [3-^{14}C] HMG CoA[2].

$$\text{HMG CoA} + 2\text{NADPH} + 2H^+ \longrightarrow \text{Mevalonate} + 2\text{NADP}^+ + \text{CoASH}.$$

Garlic disulfides were prepared by steam distillation of garlic and separated by silica gel chromatography.

3. Results and conclusions

(a) *Garlic disulfides:* Rat hepatic microsomal HMG CoA reductase was inhibited by diallyldisulfide obtained from garlic in a concentration-dependent manner, 0·5mM causing 50% inhibition. The inhibited activity was partially restored by the −SH compound DTT which afforded complete protection to the enzyme when added before inhibitor. Under similar conditions the substrate HMG CoA offered partial protection. A partially purified (50 KDa) preparation of the enzyme was also inhibited by the disulfide compound (Fig. 1). However, the inhibition was not reversed by DTT. On treatment with the inhibitor, multimers of the enzyme were not formed; neither was the inhibitor covalently bound to the protein. The inhibition presumably resulted from intramolecular −S−S− formation by exchange.

(b) *Hydrogen peroxide:* Incubation of microsomal preparations with H_2O_2 caused a rapid inactivation of HMG CoA reductase activity, which was not radical mediated. The substrate (HMG CoA) and DTT offered partial protection from inhibition. In this case also protein dimers were not produced when the microsomal preparation was treated with H_2O_2. The modulatory action of H_2O_2 on HMG CoA reductase is consistent with the recognition of H_2O_2 as a 'physiological second messenger'.

(c) *1-Ethoxysilatrane:* The complex silicon compound, ethoxysilatrane, is a potent hypocholestrolemic

agent[3] Rats when treated with the compound showed decreased circulating levels of cholesterol and decreased activity of HMG CoA reductase in hepatic microsomes. However, the enzyme activity was not inhibited when silatrane (up to 5mM) was added to microsomes. In contrast, a soluble 58 KDa preparation which contained both the 'catalytic' and 'linker' domains of the protein was found to be sensitive to inhibition by silatrane. However, the 50 KDa preparation which was devoid of the linker region was insensitive to inhibition by the compound. The results highlighted the role of the linker region in the regulation of the enzyme.

(d) *Ubiquinone:* Ubiquinone is the second major end product of the mevalonate pathway[4]. Dietary supplementation with ubiquinone has been shown to cause decreases in hepatic cholesterologenesis and serum concentration of the lipid. The activity of HMG CoA reductase measured in microsomal preparations isolated from the livers of rats fed with ubiquinone (0·5mg/rat/day for 20 days) showed a 40% decrease. The quantity of enzyme protein, however, was not decreased in the membranes.

References

1 RAMASARMA, T — *Current topics in cellular regulation*, Vol 6, 1972, pp 169-207, Academic Press.

2 SHAPIRO, D. J., NORDSTORM, J. L. MITSCHELEN, J. J, RODWELL, V. W. AND SCHIMKE, R T. — *Biochim Biophys Acta*, 1974, **370**, 369–377

3 MEHTA, P P, RAMASARMA, T. AND KURUP, C. K. R. — *Biochim. Biophys Acta*, 1987, **920**, 102–104

4 KRISHNAIAH, K V., JOSHI, V C AND RAMASARMA, T. — *Arch. Biochem Biophys.*, 1967, **121**, 147–153.

Thesis Abstract (Ph.D.)

Serine hydroxy methyltransferase from mung bean (*Vigna radiata*) seedlings: A new pyruvoyl enzyme by N. Sukanya.
Research supervisors: N. Appaji Rao and H. S. Savithri.
Department: Biochemistry.

1. Introduction

Pyridoxal phosphate (PLP) is uniquely designed to catalyse a variety of reactions of amino acids. These reactions include transaminations, decarboxylations, deaminations, transaldolizations, etc. In spite of its versatility, nature has occasionally chosen other novel cofactors to replace PLP for catalysing the same reaction. Serine hydroxymethyltransferase (SHMT) is the first enzyme in the pathway for the interconversion of folate coenzymes. The enzyme, isolated from mammalian and bacterial sources was shown to contain PLP which was essential for catalytic activity[1]. The PLP status of plant SHMTs, however, remained controversial subject. The difficulties in resolving this argument were due to (a) the unavailability of homogenous enzyme preparations or (b) the instability of the enzyme.

2. Materials and methods

Mung bean SHMT was purified to homogeneity and seemed to require PLP for stability but not for catalytic activity earlier in our laboratory[2]. The objectives of this investigation were to establish: (a) whether the mung bean SHMT required PLP for its activity? and (b) if not, what was the cofactor involved in catalysis?.

3. Results and discussion

With a view of establishing the PLP status of mung bean SHMT, the enzyme was purified both in the presence and absence of PLP by ammonium sulphate fractionation, phenyl-Sepharose hydrophobic chromatography and adsorption and elution from OADS-AH-Sepharose affinity column The enzyme purified in the presence and absence of PLP had comparable specific activities (900–1200, respectively) and were electrophoretically similar. The purified enzyme had no characteristic visible adsorption spectrum expected of a PLP protein. The enzyme was inhibited by Cys (10 mM) and the activity was restored completely upon dialysis and addition of PLP did not enhance the activity further However, in the case of mammalian SHMTs, the activity was inhibited by Cys and was restored only upon dialysis and addition of PLP. The two observations together suggested that PLP may not be required for the activity of mung bean SHMT. OADS, a potent inhibitor of sheep liver SHMT, interacted with PLP at the active site of the enzyme forming a complex which had a characteristic fluorescence emission maximum at 455 nm. Upon interaction of OADS with mung bean SHMT no such fluorescent complex was observed indicating the probable absence of PLP. The amount of mung bean SHMT used was 100 times higher than sheep liver SHMT. Penicillamine interacted at the active site of PLP enzymes causing characteristic spectral changes. However, interaction of penicillamine with mung bean SHMT did not perturb the spectrum of the enzyme confirming the absence of PLP. While sheep liver SHMT lost 70% of its activity upon interaction with penicillamine (1 mM), the activity of mung bean SHMT was unaffected. The PLP spectrum of the sheep liver SHMT as expected was perturbed by penicillamine resulting in the formation of a new absorbing species with a maximum at 330 nm.

PLP has often been replaced by a carbonyl group[3] attached to the enzyme to aid in catalysis. As a first step towards detecting the presence of a carbonyl group in the enzyme, the interaction of mung bean SHMT with various carbonyl reagents was examined. Irreversible inhibition by phenylhydrazine, hydroxylamine and sodium borohydride suggested the possible presence of a carbonyl group on mung bean SHMT. Spectral analysis of the enzyme treated with phenylhydrazine showed the appearance of a peak at 315 nm characteristic of a carbonylhydrazone, lending further support to the suggestion that a carbonyl function different from PLP was present on mung bean SHMT. Using kinetic approaches, details of the inhibition by carbonyl reagents was investigated. Phenylhydrazine inhibited the enzyme in a concentration and time-dependent manner. From a plot of pseudo first-order rate constant against phenylhydrazine concentration, a second-order rate constant of 1·9 M^{-1} min^{-1} was calculated. An n value of 0·96 indicated that one molecule of phenylhydrazine reacted/active site of the enzyme. Marginal protection by Ser and Gly against inhibition by phenylhydrazine suggested that the Schiff's linkage between Ser/Gly and enzyme carbonyl group was probably disrupted by phenylhydrazine. Similar results were obtained when the inhibition by hydroxylamine, sodium borohydride and semicarbazide was examined. OADS and AAA inhibited mung bean SHMT in the micromolar range.

Radiolabelled Ser and Gly were efficiently linked covalently to the enzyme which indicated the presence of a carbonyl function in the primary structure of mung bean SHMT. The inability of non-cognate amino acids to efficiently label the enzyme suggested that the carbonyl group was present at the active site of the enzyme to aid in anchoring the substrate/product amino acid. The above hypothesis was supported by labelling mung bean SHMT with FL-$NHNH_2$ and visualing the protein as a fluorescent band upon SDS–PAGE electrophoresis sheep liver SHMT did not yield a fluorescent band. Having shown that a covalently linked carbonyl moiety aided in the catalytic function of mung bean SHMT, it was necessary to identify the nature of the carbonyl moiety. Towards this goal the carbonyl moiety on mung bean SHMT was modified with phenylhydrazine and 2, 4-dinitrophenylhydrazine (2, 4-DNPH) separately. The modified enzyme was hydrolysed, the hydrazone extracted into ethyl acetate and identified as a pyruvoylhydrazone both by TLC and HPLC methods. Authentic α-keto acid hydrazones were chromatographed for comparision. The 2, 4-DNPH of the enzyme carbonyl group was reductively cleaved and the resulting amino acid identified as alanine, substantiating the identification of the pyruvoyl group on mung bean SHMT. The carbonyl group on mung bean SHMT was identified as pyruvate by converting it to N-(carboxyphenyl) alanine using PABA. Conclusive evidence for the presence of pyruvoyl moiety on mung bean SHMT was obtained by sodium borotritide reduction of the pyruvoyl group to the corresponding alcohol and identification of the resulting lactate by paper chromatography.

Precedence for the presence of the pyruvoyl group at the N-terminus of pyruvoyl enzymes aroused the interest to examine the site and mode of attachment of the pyruvoyl moiety on mung bean SHMT. The peptide harboring the pyruvoyl group was specifically isolated by labelling the enzyme protein with 2, 4-DNPH. The spectral characteristic of the resultant 2, 4-DNPH served as a monitoring handle to purify the peptide-containing pyruvoyl group. Employing two different strategies, namely, (a) chymotryptic cleavage, and (b) CNBr digestion followed by chymotryptic cleavage and for fragmenting the reduced and carboxymethylated protein, peptides amenable for sequencing were obtained. The peptide containing 2, 4-DNPH was purified by HPLC using TSK G 2000 SW and RP 18 columns. The purified peptide was sequenced by DABITC/PITC double coupling method. The first cycle of derivatization and cleavage did not yield any amino acid residue indicating that the pyruvoyl group was present at N-terminus of the peptide. The amino terminal block was removed by reductive cleavage resulting in the conversion of the pyruvoyl 2, 4-DNPH to Ala. In subsequent cycles of sequencing the following primary structure was obtained: (Pyr) Ala-His-Gly-Pro-Val-Ile/Leu-His-Phe-amino acid analysis revealed that the peptide contained 13 residues. However, unambiguous identification beyond the 8th residue was not possible. Based on the sequence analysis (present work) and on chemical modification studies by earlier workers the functional amino acids of the active site were envisaged and a probable mechanism of catalysis proposed.

The mechanism envisaged involves the following steps: The pyruvoyl moiety anchors the substrate, Ser, through a Schiff's linkage. The binding of Ser is facilitated by ionic interactions with Arg. Transfer of a proton from the hydroxyl group of Ser to the imidazole ring of His results in a protonated His. The resultant alkoxide is readily cleaved at the C–C bond, and the formaldehyde formed is transferred to H_4 folate. The return of the proton from His to the product Gly and release of the products by subsequent hydrolysis completes the reaction. The results presented demonstrated for the first time that a pyruvoyl moiety linked to the primary structure of SHMT facilitates the transfer of hydroxymethyl group. In other words, this work identifies mung bean SHMT as a new pyruvoyl enzyme.

References

1. APPAJI RAO, N, RAMESH, K. S., MANOHAR, R, RAO, D N., VIJAYALAKSHMI, D. AND BASKARAN, N — *J. Sci. Ind Res.*, 1987, **46**, 248–260
2. RAO, D. N. AND APPAJI RAO, N. — *Pl. Physiol.*, 1982, **69**, 11–18.
3. RESSEI, P. A AND SNELL, E E. — *A. Rev. Biochem.*, 1984, **53**, 357–387.

Thesis Abstract (Ph.D.)

Molecular modelling studies on the specificity and mechanism of action of T4 lysozyme

by P. Lakshminarasimhulu.
Research supervisor: V. S. R. Rao.
Department: Molecular Biophysics Unit.

1. Introduction

T4 lysozyme is produced late in the infection of *E.coli* by bacteriophage T4. It hydrolyzes the peptidoglycan in the cell wall and releases the progeny-phage particles. It is a beta-(1-4)-endo-acetylmuramidase like hen egg white lysozyme. But T4 lysozyme has no sequence homology with hen egg white lysozyme; nevertheless, the three-dimensional backbone structures of the two enzymes can be superimposed. The catalytic amino acid residues which take part in hydrolysis, *i.e.*, glutamic acid which donates a proton and aspartic acid which stabilizes the oxocarbonium ion intermediate are conserved and occupy identical positions in both the enzymes. The pioneering X-ray crystallographic studies of Matthews and coworkers[1] on

T4 lysozyme and its complexes with (GlcNAc) oligomers showed that the interactions of (GlcNAc) oligomers with T4 lysozyme have many similarities to those in the case of hen egg white lysozyme. It is known that (GlcNAc) oligomers or chitin fragments bind strongly to T4 lysozyme In spite of these similarities, there are marked specificity differences between T4 and hen egg white lysozymes. (GlcNAc) and (GlcNAc–MurNAc) oligomers, which are good substrates and inhibitors for hen egg white lysozyme are neither substrates nor inhibitors of T4 lysozyme. T4 lysozyme requires at least part of the peptide segment of the peptidoglycan for the hydrolysis as well as inhibition[2-3]. It is 250 times more active on *E.coli* cell walls than hen egg white lysozyme T4 lysozyme is sensitive to the substitution on the alpha-carboxyl of D-glutamic acid of the peptidoglycan. It is 1400 times more active on gram-negative *E.coli* which has no substitution on the alpha-carboxyl of D-glu than on gram-positive *M. leutus* which has a glycine substituted at the alpha-carboxyl of D-glu. In the present study an attempt was made (i) to explore the origin of specificity of T4 lysozyme, *i.e.*, to find the probable factors responsible for the inactivity of T4 lysozyme against (GlcNAc) and (GlcNAc–MurNAc) oligomers, (ii) to explain the differences in the activity of T4 lysozyme on *E.coli* and *M.leutus* peptidoglycan fragments, (iii) to determine the three-dimensional structure of the peptidoglycan from the interactions of the peptidoglycan fragments with T4 lysozyme, and (iv) to assess the extent of distortion of saccharide ring in the D site and examine the applicability of catalytic mechanisms of hen egg white lysozyme to the case of T4 lysozyme.

2. Method

A three-step molecular modelling method has been used to study the interactions of T4 lysozyme with (GlcNAc), (GlcNAc–MurNAc) oligomers and peptidoglycan fragments. The steps are:

(i) Determination of the stereochemically allowed orientations of a saccharide residue in the C site using rigid body rotation and contact criteria.

(ii) Potential energy minimization of monosaccharide–enzyme complexes (the monosaccharide is placed in all the allowed orientations) in torsion angle–rigid body parameter space. Extension of the monosaccharide in the active site to $(GlcNAc)_6$, $(GlcNAc–MurNAc)_3$, disaccharide–pentapeptide, tetrasaccharide–pentapeptide and hexasaccharide–tripentapeptide by adding saccharide residues and peptide segments to the monosaccharide.

(iii) Energy minimization of the complexes of T4 lysozyme with $(GlcNAc)_6$, $(GlcNAc–MurNAc)_3$ and hexasaccharide–tripentapeptide in Cartesian coordinate space, where all bond lengths, bond angles and torsion angles are varied.

3. Results and discussion

The present study reveals that $(GlcNAc)_3$ can bind to T4 lysozyme in four distinct modes of binding. They are labelled as normal, slant, reverse and reverse-slant modes depending on their orientation in the active site. $(GlcNAc)_6$ can bind to T4 lysozyme in normal, slant and reverse modes only. The normal mode of binding can be termed as a productive mode of binding, since the scissile glycosidic bond is near the catalytic amino acid residues. The slant and reverse modes of binding are nonproductive modes because in these modes of binding the scissile glycosidic bond is in a wrong orientation with respect to the catalytic amino acid residues. A binding mode which is similar to the slant mode is observed in the case of oxindolealanine-62 hen egg white lysozyme–$(GlcNAc)_3$ complex. The nonproductive modes of binding are energetically more favourable compared to the productive mode of binding. This may be an important factor for the inactivity of T4 lysozyme against (GlcNAc) oligomers.

$(GlcNAc–MurNAc)_3$ can bind to T4 lysozyme in normal and reverse modes. In this case also the reverse mode, which is a nonproductive mode is energetically highly favourable compared to the productive mode. This may explain the inactivity of T4 lysozyme on $(GlcNAc–MurNAc)_3$.

The pentapeptide part of the disaccharide–pentapeptide assumes many novel conformations in the active site of the T4 lysozyme. A doubly bent T shape for the pentapeptide seems to be an attractive candidate to explain the layer-like structure of *E.coli* peptidoglycan. In the doubly bent T structure the alpha-carboxyl of D-glu of the pentapeptide is directed towards the hairpin loop contacting Arg-137. Any substitution at

this alpha-carboxyl group gives rise to unfavourable steric and electrostatic interactions with the protein. This explains the differences in the activity of T4 lysozyme on *E coli* and *M.leutus* peptidoglycan segments. It is also in agreement with the hypothesis proposed by Matthews and coworkers[5] to explain the differential activity of T4 lysozyme on *E.coli* and *M.leutus* peptidoglycan segments. In the case of hexasaccharide–tripentapeptide–T4 lysozyme complex, the gross shape of the three pentapeptides emanating from B, D and F sites is similar and can be described as doubly bent antenna structures but they differ from each other in some respects.

Energy minimization studies in torsion angle–rigid body parameter space show that a saccharide ring can be accommodated in the D site without distortion. But, energy minimization studies in Cartesian coordinate space show that the saccharide ring in D site is slightly deformed but not to the extent of a half-chair or sofa conformation. The carboxylate group of Glu-11 can form hydrogen bonds with both ring oxygen and the glycosidic oxygen of the D ring with the geometry of the hydrogen bonds dependent on the orientation of the hydroxymethyl group of the D ring. The relative orientation of D and E rings is such that the lone pair orbitals on the glycosidic oxygen are not antiperiplanar to the C1-05 bond of the D ring. Because of these factors, the Post and Karplus[5] mechanism of hydrolysis of hen egg white lysozyme may not hold good for T4 lysozyme.

A comparison of the fluctuations of the main chain atoms (determined from the thermal parameters by Matthews and coworkers) of T4 lysozyme with the main chain coordinate deviations between the native and ligand-bound enzymes derived from the present study reveal interesting correlations. Thus, the main chain coordinate deviations triggered by the productive mode of binding show better correlation with the atomic fluctuations derived from X-ray thermal factors than the nonproductive modes of binding.

References

1. ANDERSON, W F., GRUTTER, M G , REMINGTON, S J. AND MATTHEWS, B. W. — *J. Mol. Biol*, 1981, **147**, 523–543
2. MIRELMAN, D., KLEPPE, G. AND JENSEN, H. B — *Eur J. Biochem.*, 1975, **55**, 369–373.
3. JENSEN, H. B., KLEPPE, G., SCHINDLER, M. AND MIRELMAN, D — *Eur J Biochem*, 1976, **66**, 319–325
4. GRUTTER, M. G. AND MATTHEWS, B. W — *J. Mol. Biol.*, 1982, **154**, 525–535.
5. POST, C. B. AND KARPLUS, M. — *J Am. Chem. Soc.*, 1986, **108**, 1317–1319.

Thesis Abstract (Ph.D.)

Vegetative and reproductive phenology of a tropical dry deciduous forest, southern India by K. S. Murali.
Research supervisor: R. Sukumar.
Department: Centre for Ecological Sciences.

1. Introduction

The present study describes the basic patterns of vegetative and reproductive phenologies of a seasonal tropical dry deciduous forest in southern India and attempts to relate these to both proximate factors and ultimate forces that may have shaped these patterns. It also draws similarities and differences between the observed patterns with studies elsewhere in tropical dry forests.

Two sites were selected to compare the differences in phenology of habitats in Mudumalai wildlife sanctuary, Tamilnadu. About 283 trees in Site I and 167 trees in Site II belonging to 38 and 27 species,

respectively, at Site I and Site II were tagged and observed at every 15-day interval. Data on stages of leaf, flower and fruit were collected on each tree. In addition, herbivore damage estimated as per cent damaged leaves was also collected. The observations were done from April 1988 to August 1990. Insect phenology data were also collected between January 1989 and March 1990 using Modified Rothemsted light traps.

2. Vegetative phenology

Shedding of leaves begins soon after the rains withdraw; this is similar to patterns observed in most seasonal tropical deciduous forests and is presumably an adaptation to conserve moisture during the dry season[1]. Leaf flushing, however, begins during the dry spell itself, well before the onset of rains in the study area. While similar observations have been reported in some neotropical dry forests, most other studies indicate that flushing is a response to the onset of rains[2,3]. Flushing during the dry season seems to be an adaptation of young tender leaves to escape from herbivorous insects that emerge later with the rains. Individuals that flushed late in the season suffered higher levels of herbivore damage to young and mature leaves as compared to those that flushed early. Thus, rainfall itself is not a proximate cue to flush leaves and trees may have mechanisms for storing water or tapping ground water for certain basic physiological functions.

3. Reproductive phenology

The peak in dry season flowering reported in certain other tropical dry forests was not necessarily true of the study area. The wetter study site did show a peak in the frequency of species flowering before the onset of rains. However, in the drier study site there was a clear pattern of wet season flowering. The rarer species tended to flower earlier in the season (drier months) as compared to the more abundant species. This could be related to the need for rarer species to avoid competition for pollinators with their abundant neighbours and also avoid the risk of heterospecific pollen deposition. A majority of species flushed leaves and flowered at the same time, thereby implying that competition between two physiologically active sites within an individual may not be a serious constraint as suggested by other observers[4].

Pollination guilds showed differences with respect to timing of flowering. Bird-pollinated trees flowered only during the dry months and these could be related to the need for better advertising their large, brightly coloured flowers during the leafless phase of the individuals. Wind-pollinated trees flowered during the wet months when wind speeds were also at their highest. However, insect-pollinated species did not show clear seasonality in flowering.

The overall fruiting phenology showed patterns whose adaptive significance was not clear in most instances. Animal-dispersed species with fleshy fruits fruited mainly during the wet months; thus moisture may be essential to maintain turgor presence in fruits. Explosive-dispersed species fruited mainly during the dry season when low relative humidity may have been necessary for their dehiscence. I did not investigate the role of fire in fruit dispersal.

There were indications that stabilizing selection would be operating as the timing of reproductive events in plants. In two out of three species studied, the rates of insect visitation on flowers, the number of pollen deposited on stigma, flower–fruit ratio, and seed number per fruit showed higher values in individuals that flowered during the mid-flowering period of the population than in those that flowered earlier or later. This implies that individuals flowering in synchrony during the mid-period of the population's flowering may also enjoy higher reproductive success.

The community of trees in a tropical dry deciduous forest thus seem to show phenological patterns that could be adaptive responses to various abiotic and biotic factors in their environment.

References

1. FRANKIE, G. W., BAKER, H. G. AND OPLER, P. A. Comparative phenological studies of trees in tropical wet and dry forests of lowlands of Costa Rica, *J. Ecol.*, 1974, **62**, 881–893.

2 PRASAD, S. N AND HEGDE, M. Phenology and seasonality in a tropical deciduous forest of Bandipur, South India, *Proc Indian Acad. Sci. Pl. Sci*, 1986, **96**, 121–133.

3 LIEBERMAN, D Seasonality and phenology in dry forests of Ghana, *J Ecol*, 1982, **70**, 791–806

4. JANZEN, D H. Synchronization of sexual reproduction of trees within the dry season in Central America, *Evolution*, 1967, **21**, 620–637.

Thesis Abstract (Ph.D.)

Local variation and base sequence effects in nucleic acid structures by Dhananjay Bhattacharyya.
Research supervisor: Manju Bansal.
Department: Molecular Biophysics Unit.

1. Introduction

Determination of the molecular structure of nucleic acid fragments has reached a level that one can think of understanding details of sequence-directed structural features from the available data. Such analyses had been started[1,2] nearly a decade ago on the basis of only two or three crystal structures of oligonucleotide fragments determined by X-ray analysis and the theories were based on a detailed examination of very limited data. Due to the availability of several more X-ray single-crystal structures, energy-minimized model structures based on X-ray fiber data and also models based on two-dimensional NMR data, it is now easier to understand sequence-dependent effects.

2. Method

The structural variations can be understood well from the stacking arrangements of the constituent basepairs, rather than the backbone torsion angle values, but such an analysis is difficult for non-regular nucleic acid double-helical molecules using any of the available methodology. The basepairs in a nucleic acid structure, being nearly planar, undergo least amount of distortions and are relatively insensitive to the procedure followed for structure determination. Hence, an analysis of basepair orientation is more suitable to pinpoint any structural variability. However, no algorithm was available to analyze the relative orientation of the basepairs, *i.e.*, the basepair parameters, from a completely local point of view.

A self-consistent algorithm for analysis and generation of nucleic acid structures was therefore developed to meet these requirements. It is known that three rotational and three translational parameters are required to completely specify relative orientations of two rigid bodies. Following the convention proposed at the EMBO Workshop on DNA Curvature and Bending, held at Cambridge, UK, in 1988[3], three independent rotational parameters have been defined as tilt, roll and twist. Similarly, the three translational parameters defined are shift, slide and rise. However, for describing the intra-basepair orientation three rotational parameters, *viz.*, propeller twist, buckle and opening angle and only one translational parameter, *viz.*, C8 . . . C6 distance have been defined, which are seen to be reasonably sufficient for characterizing relative orientation of two planar objects. The proposed algorithm has been tested for self-consistency by regenerating several available crystal structures from their local parameter values and the root mean square deviations between the actual and the regenerated structures are found to be very small.

3. Results

(i) Base sequence effects in DNA crystal structures

A detailed analysis of the fiber models has been carried out in terms of the above-mentioned local doublet parameters. Three-dimensional coordinates of crystal structures of double-helical DNA that are available

in public domain have also been analyzed to understand the sequence and environment effects on B-DNA and A-DNA double helices. No strong sequence effect is observed in B-DNA crystal structures, while the basepairs of the pyrimidine–purine doublet sequences are found to roll open towards the minor groove in A–DNA crystal structures. The purine–pyrimidine and purine–purine doublet sequences in A–DNA, however, have much smaller roll angle compared to the A-DNA fiber models Similar sequence-dependent effects are also observed in the duplex regions of tRNA crystal structures as well as the energy minimized dinucleoside monophosphate structures in A-form. Though the local doublet parameters are shown to be extremely powerful in understanding sequence-dependent structural features in oligonucleotides, they are not clearly related to the gross structural parameters of DNA. Attempts have been made to understand several gross structural features of nucleic acids from the local parameters. A comparative analysis of the two different forms of nucleic acid duplexes, *viz.*, A-form (including A-DNA and double helical regions of tRNA) and B-form, indicate that slide and to some extent roll are the only local doublet parameters which distinguish between the two forms of structures in oligonucleotide crystals.

(ii) Base sequence effects in tRNA crystal structures

The tertiary fold of two tRNA, *viz.*, $tRNA^{Phe}$ and $tRNA^{Asp}$ has also been analyzed on the basis of intra-basepair and local doublet parameters to verify the applicability of the local parameters. The five $tRNA^{Phe}$ crystal structures solved under different environmental conditions and crystallized in different space groups show some differences in the values of intra-basepair and local doublet parameters, though the general trend of values is similar. However, in the D-stem the local doublet parameters are very much conserved in all the five structures, indicating the importance of this region in tRNA recognition, since sequence of the D-stem is also conserved in all the available $tRNA^{Phe}$ sequences of different species.

(iii) Local doublet parameters control minor groove width of DNA double helices

It has also been shown that slide has the strongest effect on the minor groove width of B-DNA structures, while roll and twist are the other local parameters weakly affecting the groove size of B-DNA structures. Thus, the slide parameter (which is related to the more commonly used parameter), x-displacement, of the basepairs from the helix axis) is shown to be the most important in characterizing gross features of nucleic acid structures.

(iv) Understanding DNA bending using local doublet parameters

A quantitative estimate has also been made of axial curvature in oligonucleotide structures using several different methods. It has been shown that none of the methods, except those making use only of the first and last basepair orientations (and hence similar to the procedure followed in NEWHELIX90) give curvature values as reported earlier for the B-DNA dodecamer crystal structure of sequence d(CGCGAATTCGCG). The well-known methods, such as fitting of a plane curve or sphere to the local helix origins, give absurdly small values for radii of curvature in all the structures. An alternative estimate is made from an examination of the path traced by the local helix axes. The angle between the first and the last helix axes is quite small for all the crystal structures, indicating that there is no significant curvature in any of the structures. Thus, a perturbation in the basepair orientation in an oligonucleotide does not necessarily lead to the molelcule being really curved, though it may appear curved. The above procedures using local helix axes or origins can be applied to a nucleotide sequence of any length. Its application to polymeric structures, with different stretches of oligo As in the middle of a decamer repeat, give values identical to those obtained from the decamer repeats, thus proving the general validity of these methods.

(v) Base sequence-dependent structural variations explain DNA bending

The mean value of each local parameter is quite different for various doublet sequences even though no strong sequence-dependent structural feature is observed in the B-DNA crystal structures, unlike the case of A-form structures. Thus, an attempt has been made to understand some of the observed structural features of DNA fragment using the mean parameters. For example, the experimental observation of certain natural and synthetic sequences moving anomalously slowly in polyacrylamide gel has been attributed to intrinsic bending of these molecules. Therefore, several such polynucleotide sequences have been generated using the mean parameters obtained for B-DNA as well as A-form crystal structures. It is found

that most of the sequences, which move abnormally in the gel, are more curved when those are generated using the mean paramters of B-form as well as A-form crystal structures while the sequences which move normally are generally straight. This probably indicates that any systematic variation in the roll angles leads to certain base sequences to be intrinsically curved, though there may be differences in the precise path traced by the molecule.

References

1. CALLADINE, C. R. — *J Mol. Biol.*, 1982, **161**, 343–352.
2. DICKERSON, R E. — *J Mol. Biol.*, 1983, **166**, 419–441
3. DICKERSON, R. E , *et al* — *J. Mol. Biol* , 1989, **205**, 787–789; *EMBO J* , 1989, **8**, 1–4; *J Biomol. Struct. Dynam.* 1989, **6**, 627–634

Thesis Abstract (Ph.D.)

Studies on the DNA binding and specificity of some synthetic nonintercalators by Devapriya Choudhury.
Research supervisors: V. Sasisekharan and M. Bansal.
Department: Molecular Biophysics Unit.

1. Introduction

The interaction of double-stranded DNA (ds-DNA) with the oligopeptide antibiotics Netropsin (Nt) and Distamycin-A (Dst) have been the subject of intense research in recent years. Nt and Dst-A are both antibiotics synthesised by *Streptomyces netropsis* and *S. distallicus*, respectively, and bind to ds-DNA in the B-form. They show a strong preference for the minor groove and AT base pairs. The exact binding mechanism of these compounds and the reasons for their high specificity remains obscure despite tremendous amount of work[1].

It was earlier proposed from this laboratory[2] that intrinsic curvature of the ligand backbone may have a role to play in the DNA-binding activity of these and related compounds. In order to test this concept a related set of compounds have been designed which vary in the intrinsic backbone curvature to a large extent. Comparison of the binding activities of the compounds were expected to show whether intrinsic curvature does indeed have an important role to play in DNA binding or not.

2. Methods

Design of the compounds was based on the isohelical analysis approach pioneered by Goodsell and Dickerson[3]. In this method, the backbone of an infinite helical polymer is generated and its conformation varied to match that of B-DNA. Those conformations whose helical parameters matched those of B-DNA were judged to be suitable for binding and were termed 'isohelical' conformations.

Solution-phase syntheses of the peptide ligands were carried out by classical techniques employing the reaction of an acyl chloride with an amine to generate the peptide bond. Terminal amidine moiety was generated by pinner reaction of the corresponding nitriles. Since the compounds were achiral this method afforded convenient separation of the products from the reaction mixtures. The identity of all the compounds including the synthetic intermediates was confirmed by IR and ^{1}H-NMR spectra and by elemental analysis. The purity of the final compounds was checked by reverse-phase HPLC.

Physicochemical studies were carried out mainly by CD spectroscopy using a Jasco J-500A spectropolarimeter coupled to a DP501 data processor. UV melting profiles were determined using a Beckman DU8B spectrophotometer coupled to a thermoprogrammable Tm cell holder. Melting data were analysed by a program written by the author using the MATLAB software package. UV spectral titrations and

kinetics were also carried out on the Beckman DU8B spectrophotometer with software supplied by the manufacturer.

Diffraction data were collected in a CAD4 four-circle diffractometer and the structures were solved and refined using the SHELEX 400 program package. The final structures were visualised by a program written by the author and interfaced to the molecular graphics package DTMM.

Molecular mechanics calculations on the ligand-DNA complexes were performed using AMBER 3·0. The nucleic acid portion of the energy-refined complexes was analysed out using the program NUPARM and the final structures visualised by DTMM. Prior to molecular mechanics refinement, the ligands were interactively docked on to the DNA molecule using the DTMM package.

3. Results

Isohelical calculations showed that any ligand comprising alternately linked meta- and para-substituted benzenes would have conformations suitable for DNA binding; however, those compounds which were made up of consecutive blocks of meta- or para-substituted benzenes would not be suitable for DNA binding. In order to test this concept, five compounds were synthesised. Three of them had alternating meta- and para-substituted benzene rings while the other two were solely made up of meta- or para-substituted benzene rings. Two of the three isohelically suitable compounds had a terminal nitro group while the third one had an additional benzamide group instead of the nitro group.

Physicochemical studies showed that only the three isohelically favourable ligands could bind to DNA, while the other two did not show any measurable binding effect with DNA. Among the compounds which bound to DNA, the ones with a terminal nitro group showed very high specificity for AT base pairs and bound to natural DNA polymers only if the AT content in those polymers was higher than 80%. The third compound which lacked the nitro group and comprised of an additional benzamide group was also AT specific, but to a lesser extent and could bind to natural DNAs having $\approx$ 60% AT content. All the three compounds were specific for the minor groove of B-DNA and did not bind to RNAs or A-form DNA.

X-ray crystallographic study of three compounds related to the ligands was carried out. These compounds possessed the same aromatic backbone as that of the ligands, but lacked the charged end groups. Examination of the final refined structures showed that even though the compounds were not truly isohelical in the crystal, they nevertheless shared the characteristics thought to be important in DNA binding, *viz.*, having a curved shape with the peptide NHs pointing in the concave direction. It was also observed that the crystal conformation is most likely the result of intermolecular aromatic–aromatic stacking interaction in the crystal. This indicated that the compounds were flexible enough to take up isohelically suitable conformation in the minor groove of DNA.

Detailed molecular mechanics calculations were performed with one of the DNA-binding compounds, *viz.*, 3-(4-(3-nitrobenzamido) benzamido) propionamidine hydrochloride complexed with a series of oligonucleotide decamers with repeating sequences. Complexes where the ligand is bound either along the minor and the major grooves of the oligonucleotides were taken up for study. From the calculated interaction energies obtained from the molecular mechanics studies, conclusions could be drawn about the AT base pair and minor groove-binding preference of the test compound and these were found to be in excellent agreement with the experimentally observed trends. Further calculations were then performed on the minor groove complexes of the ligand with the oligonucleotide d(CGCGAATTCGCG)$_2$. The oligonucleotide model used in these complexes was either generated from fibre diffraction data, or taken from the single-crystal structure solved earlier by Dickerson and coworkers[4]. It was observed that the ligand bound better to the crystal model than to the fibre model of the oligonucleotide. Additionally an 'induced fit' type of binding was observed for the ligand and the fibre model oligonucleotide, but not for the crystal model oligonucleotide. Taken together, the results from molecular mechanics calculations pointed to an interplay of steric and electrostatic factors which determine the highly specific interaction of this ligand and DNA.

References

1. ZIMMER, C. AND WAHNERT, U. *Prog. Biophys Mol. Biol*, 1986, **47**, 31–112.
2. RAO, K. E., DASGUPTA, D. AND SASISEKHARAN, V. *Biochemistry*, 1988, **27**, 3018–3024
3. GOODSELL, D. AND DICKERSON, R. E. *J. Med. Chem.*, 1986, **29**, 727–733.
4. DREW, H. R AND DICKERSON, R E. *J Mol. Biol*, 1981, **151**, 535–556.

Thesis Abstract (Ph.D.)

DNA polymerases of the silkworm *Bombyx mori* by S. Niranjanakumari.
Research supervisor: K. P. Gopinathan.
Department: Microbiology and Cell Biology.

1. Introduction

Extensive research in the field of DNA replication has one common goal, *viz.*, to understand how the duplication of the genetic meterial is achieved and how is it regulated? Several model systems (*E. coli* DNA polymerase III and SV 40 and yeast systems) have helped to come closer to this aim. Although these model systems have led to considerable increase in knowledge of the DNA replication, the aspects of coordinate functions of DNA polymerases and their accessory proteins at the replicative fork still remain elusive. The present investigation was undertaken in this context.

2. Results

The silk gland of *B. mori*, a terminally differentiated tissue undergoes chromosomal endoduplication throughout larval development[1]. The DNA content as well as DNA polymerase activity in the middle and posterior silk glands on different days of larval development were examined. The DNA level increases by 300,000 times the haploid genomic content amounting to 18 rounds of replication in the posterior silk gland. The DNA doubling time is approximately 48 and 24 h during the fourth and fifth instars of larval development, respectively. However, it does not change during the interim molt. This strategy rather than specific gene amplification is adopted by the silk glands to achieve an increase in gene copy number.

Concomitant with increase in DNA content, DNA polymerase α and δ activities also increase as the larval development progresses. Both polymerase α and δ are tightly associated with the nuclear matrix. The increasing levels of both DNA polymerases in parallel to the increase in DNA content and their strong association with the nuclear matrix suggest a definite role for these enzymes in chromosomal DNA replication.

DNA polymerase α from the silk gland extracts was purified to homogeneity using a series of conventional as well as affinity chromatographic techniques. The M_r of the native enzyme was found to be 560 kDa. The enzyme is a heterogeneous multimer comprising six non-identical subunits of 180, 140, 110, 55, 45 and 27 kDa and the catalytic activity is resident in the 180 kDa subunit. The enzyme shows a pI of 6·2 and the Km values for dNTP vary from 5 to 16 μM. The native DNA partially digested with DNase I or synthetic poly(dA)·$(dT)_{12-18}$ was found to be excellent template for DNA synthesis. Polymerase α has an intrinsically associated primase activity which initiates primer synthesis in the presence of rNTPs on an ssDNA template. The primase activity is resident in the 45 kDa subunit[2].

In addition to polymerase α, polymerase δ is also present in large quantities in silk gland cells. This enzyme was purified to homogeneity and its identity as distinct from DNA polymerase α or other polymerases has been established. Polymerase δ possesses $3' \rightarrow 5'$ exonuclease activity which functions

Table I

Properties of DNA polymerases* from *B. mori*

Property	*DNA polymerase (α)*	*DNA polymerase (δ)*	*DNA polymerase (ϵ)*	*DNA polymerase (β)*
Optimum pH	8·5	6·5	6·5	8·5
Native M_r	560,000	300,000	n.d	40,000
No. of subunits	6	3	2	1
(M_r kDa)	(180, 140, 110, 55, 45 & 27)	(170, 70 & 42)	(215 & 42)	(40)
Associated activity	Primase	3′ → 5′ exonuclease	3′ → 5′ exonuclease	
Effect of auxiliary protein	No effect	Stimulation	No effect	nd
Sensitivity to inhibitors				
Aphidicolin	Inhibition	Inhibition	Inhibition	No effect
NEM	Inhibition	Inhibition	Inhibition	Partial inhibition
ddTTP	No effect	nd	nd	Inhibition
BuPhdGTP	Inhibition	No effect	No effect	nd
BuAndATP	Inhibition	No effect	No effect	nd
DMSO	Stimulation	Stimulation	Inhibition	nd
Polymerase α antibody	Inhibition	No effect	No effect	No effect
Polymerase δ antibody	No effect	Inhibition	Partial inhibition	nd

* : DNA polymerase α, δ and ϵ were purified from the silk glands of *B.mori* and DNA polymerase β was purified from the pupal ovaries of *B mori*

nd· Not determined

effectively in proofreading during DNA synthesis. The processivity of this enzyme during catalysis is enhanced by an auxiliary protein analogous to proliferating cell nuclear antigen which has also been purified to homogeneity from silk glands[3].

The DNA repair process, which is also a part of DNA replication, is known to involve the participation of DNA polymerase β, but this enzyme is absent in the silk glands. However, DNA polymerase β activity could be demonstrated in the gonadal tissues of *B. mori*. Since the silk gland cells are devoid of DNA polymerase β, a search for other enzyme which could function in repair was carried out which led to the identification of DNA polymerase ϵ, recently implicated enzyme in DNA repair.

DNA polymerase β from the pupal ovaries and ϵ from the silk glands were also purified and characterized. The former enzyme satisfied the criteria to be designated as polymerase β based on its small size, sensitivity to ddTTP and insensitivity to aphidicolin. It is a monomeric polypeptide of M_r 40 kDa. DNA polymerase β is biochemically and immunologically distinct from polymerase α and δ. The absence of the associated primase and exonuclease activities and its conspicuous absence in highly replicative tissue imply that it is unlikely to participate in the DNA endoduplication process[4]. On the other hand, DNA polymerase ϵ is a heterodimer of 215 and 42 kDa subunits. It resembles DNA polymerase δ, in having intrinsic 3′ → 5′ exonuclease activity, sensitivity to aphidicolin and resistance to BuPhdGTP and BuAndATP. However, it could be readily distinguished from polymerase δ by its insensitivity to the auxiliary protein (*viz.*, PCNA) and inhibition by DMSO. DNA polymerase ϵ showed partial immunological crossreactivity with polymerase δ, but had no relatedness with polymerase α and β. The properties of all the four DNA polymerases are summarized in Table I.

3. Conclusions

The abundant presence of DNA polymerase α and δ in the silk gland and the corresponding increase of their activities with the increasing levels of DNA contents and their tight association with the nuclear matrix strongly suggest their role in chromosomal endoduplication. The absence of repair enzyme polymerase β and presence of polymerase ε suggest a possible role for this enzyme in DNA repair synthesis in the silk glands. Thus, the present investigation of DNA polymerases has opened up a new model system to study eukaryotic DNA replication.

References

1. GAGE, P. L — Polyploidization of the silk gland of *Bombyx mori*, *J. Mol Biol*, 1974, **86**, 97–108.

2. NIRANJANAKUMARI, S. AND GOPINATHAN, K. P — Characterization of DNA polymerase α-primase complex from the silk glands of *Bombyx mori*, *Eur J. Biochem.*, 1991, **201**, 431–439.

3. NIRANJANAKUMARI, S AND GOPINATHAN, K. P. — DNA polymerase δ from the silk glands of *Bombyx mori*, *J Biol. Chem*, 1992, **267**, 17531–17539.

4. NIRANJANAKUMARI, S AND GOPINATHAN, K. P. — DNA polymerase β from the pupal ovaries of *Bombyx mori*, *Insect Biochem Mol. Biol*, 1993 (In press).

Thesis Abstract (Ph.D.)

Unusual DNA structures and transcription control by Rajesh Bagga.
Research supervisor: Samir K. Brahmachari.
Department: Molecular Biophysics Unit.

1. Introduction

Structural polymorphism in DNA was envisaged from the fibre diffraction studies though all forms were believed to be monotonous right handed. However, subsequent theoretical studies suggested that the DNA helix could deviate significantly from the right-handed structure and later single-crystal x-ray studies of synthetic oligonucleotides led to speculations that such structures might have important roles in protien–nucleic acid interactions. Among the structures which received considerable attention from the structural viewpoint are cruciform, left-handed Z-DNA, bent DNA and triplexes. Unlike the usual B-DNA structure, these unusual DNA structures require a specific sequence motif and are influenced by environmental factors. Supercoiling of DNA has been found to be obligatory for the stabilization of some of these structures under physiological conditions. Characteristic exposed bases in these unusual structures were shown to be the preferred sites for single-stranded nucleases and certain chemical probes. Identification of certain proteins which recognize and stabilize these structures indicated that some of these unusual DNA structures *per se* may be the site for genetic regulation. Indeed, later studies showed that some of the *cis*-acting regulatory elements of transcription occurring in the flanking regions as well as within the genes were found to meet the necessary sequence criteria required for adopting unusual DNA structures. Identification of single-strand specific nuclease and DNase I-hypersensitive sites corresponding to these regions of the transcriptionally active genes further raised the possibility that such unusual DNA structures might be playing an important role in transcription regulation.

A topologically unlinked ($LK = 0$) highly supercoiled molecule, the form V DNA, reconstituted by annealing complementary single-stranded circles was used as a template for *E. coli* RNA polymerase for *in vitro* studies. Topological constraints require that every right-handed helical turn to be compensated by a left-handed turn or a negative supercoil. Thus, a large portion of the form V molecule is forced to adopt unusual DNA conformations. Restriction endonucleases and methylases used previously[1] showed that

unusual structures in pBR322 form V DNA are distributed both within and around the genes. Thus, pBR322 form V DNA, a natural DNA sequence, was an obvious choice for the *in vitro* studies. For the *in vivo* studies a 'structural cassette' approach was developed which involves knowledge-based design of oligonucleotide sequences having potential to adopt unusual DNA structure. The oligonucleotides were synthesized and functional assays were performed after introducing these cassettes in an appropriate expression vector either in the promoter region or within the gene. Our results show that formation of B–Z junction in the promoter region inhibits transcription initiation and occurrence of cruciform structure within the gene block transcription elongation.

2. Experimental methods

Controlled digestion of supercoiled pBR322 DNA was performed to create a single nick per molecule. The complementary single-stranded circular DNA molecules were purified from linear molecules on a 5–20% alkaline sucrose density gradient and were annealed to generate paranemically coiled form V DNA. Electroeluted form V DNA preparation was used for all the experiments. HpaII single hit analysis of the CCGG site in pBR322 form V DNA was performed by partial digestion with restrictive amounts of enzyme. *In vitro* transcription assay of the pBR322 form V DNA template and control pBR322 form I DNA template was performed with purified *E. coli* RNA polymerase (RNAP) and using either ^{3}H-UTP or α-^{32}P-UTP as labelled substrate. Transcriptional products were analysed on 10% polyacrylamide gel (PAG) containing 8·3M urea. Abortive transcription initiation assay for *rep* gene of pBR322 was carried out in the presence of only two nucleotides, *i.e.*, ATP, the initiating nucleotide and α-^{32}P-CTP as labelled substrate. Mapping of altered conformation at pause site 3045 was performed by estimating the extent of methylation in form V DNA with MspI methylase. Following recombinant plasmids were constructed by ligating synthesized oligo duplexes into an appropriate vector using T4 DNA ligase.

Plasmid pRM36 : insert was a partial ClaI digest of poly d(CGCGCGATCGAT) and cloned into unique ClaI site of pBR322. A clone with 36bp of the insert sequence was selected for various structural and functional studies.

Plasmid pRB38: a derivative of pRM36 wherein the insert region is a synthesised 69 mer oligoduplex having designed σ_{70} promoter sequence wherein −35 consensus sequence was flanked by left-handed Z-forming sequence.

5′–AATTCTCATGTAGATCTGCTTATCATCGATCGCGCGATCGATCGCGCGATTGATCGCGCGATCGATTCA
3′–GAGTACATCTAGACGAATAGTAGCTACGCGCGTAGCTAGCGCGCTAACTAGCGCGCTAGCTAAGTTCGA

Plasmid pSBC1: contains a synthesised 51 nucleotide-long oligoduplex corresponding to 5 to 22 amino acids of the pUC19 β-galactosidase gene designed using degenerate codons to have inverted repeat sequence having potential to adopt cruciform structure with 18bp stem and 4bp loop. A computer program was used for this design. This oligoduplex was replaced with original sequence of pUC19 extending from *Eco*RI to *Hind*III.

5′–AGCTTGCATGCCTGCTCGACGACACTCGAGAATCCTCGAGTGCCGTCGAGC
⟵ ⟶
3′–ACGTACGGACGAGCTGCTGTGAGCTCTTAGGAGCTCACGGCAGCTCGTTAA

Plasmid pSBmC1: contains a synthesised 51 nucleotide-long oligoduplex wherein homonymus codons for Ser, Thr and Pro occurring within the inverted repeat region were shuffled to abolish the cruciform potential of this sequence yet maintaining the identical amino acid sequence as pSBC1. Correct sequence in the insert region was confirmed by sequencing purified plasmids.

5′–AGCTTGCATGCCTGCAGCACAACGCTCGAGAATCCGCGAGTGCCTTCGTCG
3′–ACGTACGGACGTCGTGTTGCGAGCTCTTAGGCGCTCACGGAAGCAGCTTAA

Topoisomers of the recombinant plasmids were prepared by relaxing Cs-gradient purified supercoiled plasmids in the presence of different amounts of ethidium bromide with wheat germ topoisoimerase I. 2D-agarose gel (1–1·5%) was run in 1 × TBE having 1·3μM chloroquine in the second dimension. Electrophoretic mobility shift assay to elucidate left-handed Z-conformation in pRM36 and pRB38 was

performed using 0–1·05μg of monoclonal anti-Z-DNA antibody (Z-22, a kind gift from Dr. B.D. Stollar). Fine mapping of B–Z junction in supercoiled pRM36 was performed using SI nuclease. Expression of tetracycline gene was monitored by checking the sensitivity of the *E. coli* cells harbouring different recombinant plasmids in the presence of various amounts of tetracycline and from the dot blot analysis of purified RNA using tet^R gene-specific probe. Expression of the β-*gal* gene was monitored according to the Miller's assay and dot blot analysis of the purified RNA with oligonucleotide probes corresponding to 5′ and 3′ with respect to the insert region of β-*gal* gene.

3. Results and discussion

Single hit analysis of 26 HpaII sites (CCGG) showed differential cleavage efficiency of each site. The variation in cleavage efficiency could be correlated to the occurrence of sequence motifs of various unusual DNA structures present in the immediate flanking region of these sites. Occurrence of sequence motifs for the left-handed, H-form and cruciform in the flanking region reduced the cleavage efficiency and results obtained were in accordance with the structural studies performed previously in our lab[1]. Compilation of all the structural studies performed on pBR322 form V DNA indicated a direct correlation between the occurrence of an altered site in a domain with the high G/C content of that domain. To delineate the role of supercoil-stabilized unusual DNA structures in modulating the various steps in transcriptional process ability of pBR322 form V DNA to act as a template for the *E. coli* RNAP was tested *in vitro* using ^{3}H-UTP as one of the substrates[2]. Significant transcription was observed from the form V DNA template despite its high level of superhelical density Analysis of the RNA products on denaturing PAG showed the formation of only one 69 nucleotide-long transcript from form V template as compared to three different transcripts of length 110, 180 and 540 corresponding to *rep*, tet^R and amp^R gene, respectively, obtained using form I DNA template. Abortive initiation assay showed that 69 residue transcript from form V DNA template was initiating accurately from the P4 promoter of *rep* gene. This pausing could be removed by relieving the torsional stress implying that a supercoil-stabilized structural alteration within the *rep* gene was acting as a transcription elongation block. Cruciform nature of the structural block in form V DNA was confirmed from the methylation sensitivity assay. Structural studies using restriction endonucleases and methylase showed that promoter region of the tet^R gene in form V DNA comprised alternating B and non-B conformation which was correlated to the absence of tet^R gene product.

Plasmids pRM36 and pRB38 were constructed to delineate the role of supercoil-stabilized B–Z junction in the promoter region on transcription initiation *in vivo*. 2D-chloroquine gel analysis of the topoisomers, EMS assay and SI nuclease fine mapping studies of the supercoiled plasmid pRM36 and pRB38 showed that an alternating left-handed Z- and right-handed B-conformation could be stabilized after every half a turn of the helix under physiological superhelical density[3]. The tet^R-promoter region of pRM36 had a putative –35 canonical sequence and a 15bp spacer DNA separating –35 and –10 canonical sequences. The hexameric –35 canonical sequence of tet^R gene in plasmid pRB38 has four most conserved bases identical to the –35 sequence of tet^R gene in pBR322 and has optimum 17bp spacer DNA. In pRB38 and pRM36 both 5′ and 3′ flanking residues are involved in B–Z junction formation. *E. coli* cells harbouring pRB38 or pRM36 failed to grow in the presence of optimum concentration of tetracycline. At suboptimal concentration of tetracycline, however, cells harbouring pRB38 showed detectable growth implying that the designed tet^R promoter is functional. Tetracycline sensitivity was corroborated by the absence of transcription initiation from the tet^R promoter upon RNA dot blot analysis. Thus, formation of B-Z junction at the –35 canonical sequence led to transcription initiation inhibition in pRB38.

Plasmids pSBC1 and pSBmC1 were constructed to delineate the role of cruciform structure occurring within the gene in transcription elongation *in vivo*. Shift in the mobility of pSBC1 topoisomers implied extrusion of inverted repeat sequence to cruciform under physiological conditions. No such change was observed in the case of pSBmC1 topoisomers. *E. coli* cells harbouring pSBC1 gave light blue color colonies on X-gal indicator plate whereas pSBmC1 cells showed normal deep blue color colonies[4]. Miller's assay for *in vivo* β-galactosidase activity showed 10-fold lower activity in the case of cells harbouring pSBC1 as compared to cells harbouring pSBmC1[5]. 5′-Probe corresponding to β-*gal* gene hybridized equally to the total RNA purified from both pSBC1 and pSBmC1 cells. On the other hand, weak hybridization signal

with 3'-probe from pSBC1 RNA as compared to pSBmC1 RNA implied transcription elongation block caused by introduced cruciform structure within the β-*gal* gene. In conclusion, unusual structure of the template DNA *per se* provides a novel class of regulatory elements which act in *cis* to regulate transcription.

References

1. BRAHMACHARI, S K., RAMESH, N., SHOUCHE, Y. S., MISHRA, R. K. BAGGA, R. AND MEERA, G. — In *Structures and methods*, Vol. 2, (R H. Sarma and M. H. Sarma, eds), 1990, pp 33–49, Adenine Press.
2. BAGGA, R , RAMESH, N. AND BRAHMACHARI, S. K — *Nucleic Acids Res.*, 1990, **18**, 3363–3369.
3. BRAHMACHARI, S. K., MISHRA, R. K., BAGGA, R. AND RAMESH, N. — *Nucleic Acids Res.*, 1989, **17**, 7273–7281.
4. SARKAR, P. S., BAGGA, R. BALAGURUMOORTHY, P AND BRAHMACHARI, S K. — *Curr Sci* , 1991, **60**, 586–591.
5. BRAHMACHARI, S. K., SARKAR, P. S , BALAGURUMOORTHY, P., BURMA, P. K. AND BAGGA, R. — *Nucleic Acids Res. Symp. Ser.*, 1991, **24**, 163–166.

Thesis Abstract (Ph.D.)

Studies on the molecular mechanism of action of 5-fluorouracil: Interaction of aminoacyl tRNA synthetases with 5-fluorouracil-substituted transfer RNA from rat liver by A. Madan Kumar.
Research supervisor: R. Nayak.
Department: Microbiology and Cell Biology.

1. Introduction

5-Fluorouracil (FUra), a halogenated pyrimidine, is a potent anticancer drug. It has been shown to incorporate into various nucleic acids. Though the degree of antineoplastic activity of FUra is directly proportional to the concentration of its incorporation into RNA[1], the exact mechanism by which such an incorporation leads to cytotoxicity is not clearly understood. In an attempt to define the precise effect of FUra incorporation into RNA, FUra containing hnRNA[2], mRNA[3], rRNA[4], primer RNA[5] has been isolated and analyzed from various sources. However, little attention has been paid to the understanding of the effect of FUra incorporation into eukaryotic tRNA. FUra readily incorporates into tRNA replacing both uracil and uracil-derived modified bases.

In the present study, the biological role of FUra-incorporated tRNA (FUra-tRNA) was examined with respect to its interaction with aminoacyl-tRNA synthetases (AARS) isolated from rat liver.

2. Materials and methods

Total tRNA from rat liver was isolated by Zubay's method[6] and followed by gel filtration on Sephadex G-200. Similarly, FUra containing tRNA was isolated from rat liver after injecting rats with FUra (250 mg/kg) for 3 h. Further, FUra-tRNA was separated on DEAE sephacel column. A single species of tRNA (Lysyl-tRNA) was isolated from both normal tRNA and FUra–tRNA by FPLC on Mono Q.

Aminoacyl tRNA synthetases (AARS) complex was isolated from rat liver by 2–5% polyethylene glycol (PEG–8000) precipitation method. Lysyl–tRNA synthetase was purified from such a complex either by ultracentrifugation[7] or by affinity chromatography[8].

As a first step in the study of the effect of FUra incorporation into tRNA, aminoacylation reactions were carried out. Similarly, studies were extended to find out the effect of the presence of fluorine at C-5 position in FUra and fluorouridine (FURD) on hydrogen exchange reactions carried out by AARS. Further, oligonucleotide mapping of both lysyl tRNA (normal and FUra substituted) was carried out in an attempt to define the exact mode of FUra–tRNA-mediated cytotoxicity.

3. Results and discussion

Isolation of tRNA from rat liver by Zubay's method coupled with gel filtration on Sephadex G-200 yielded 6–8 A_{260} units of tRNA per gram of tissue. Analysis of tRNA isolated from FUra-injected rats indicated that approximately 76% of total tRNA was found to contain FUra. Alkali hydrolysis of such tRNA on TLC showed that approximately 47·8% of uracil bases in FUra–tRNA were replaced by FUra.

Aminoacylations of these tRNAs by AARS in the presence of various [^{14}C]-labelled amino acids showed that the efficiency of amino-acid acceptance by FUra–tRNA was decreased. Decreased levels of aminoacylations of FUra–tRNA by AARS was thought to be due to increased binding of AARS to FUra-tRNA. Kinetic studies indicated that V_{max} for FUra–tRNA was markedly decreased due to FUra incorporation indicating the formation of tight complex of AARS and FUra–tRNA.

AARS, during acylation reactions, carry out C-5 hydrogen exchange reaction with uracil located at 8th position in tRNA. Initial studies carried out with FUra and FURD indicated that AARS failed to carry out C-5 hydrogen exchange reactions because both FUra and FURD lack hydrogen at C-5 position and hydrogen is replaced by fluorine in these bases. Prolonged incubation (16 h) of FURD and URD (uridine) with AARS resulted in the release of fluorouracil and uracil, respectively, indicating that AARS carry out glycosidic bond cleavage instead of C-5 exchange. The extent of release of FUra from FURD was 3·8 folds more than that of release of uracil from URD.

Similarly, incubation of AARS with [^{3}H] FUra–tRNA resulted in the release of [^{3}H] FUra indicating that AARS could carry out 'glycosidase' activity when incubated with tRNA molecule. Further, addition of amino acids to this reaction enhanced the release. The release was found to be 2·5 folds more for FUra–tRNA than normal tRNA. This observation indicated that the process of aminoacylation enhances the susceptibility of FUra–tRNA to glycosidase activity by AARS. The partial inactivation of the enzyme by exposing it to 45°C for 1 h resulted in the decreased capacity of AARS to carry out both aminoacylation and glycosidic bond-cleavage reactions. This result suggested that both the activities have similar temperature sensitivity. Further, tRNA samples obtained after preincubation with AARS were isolated, denatured, renatured and used in the acylation reactions. Normal tRNA, after such treatments lost 30·5% of the acylation activity, whereas FUra–tRNA lost 81% of the activity. These tRNAs were analysed by 8% PAGE and found that there was considerable degradation of FUra–tRNA due to incubation with AARS. This result was further confirmed by thermal denaturation studies where preincubation of FUra–tRNA with AARS resulted in decreased T_m of FUra–tRNA (38·5°C) than normal tRNA (46·5°C).

In order to find out whether such kind of glycosidase activity is inherent to AARS or a contaminating activity, studies were carried out with a purified lysyl–tRNA and lysyl–tRNA synthetase from rat liver. After incubation of ^{32}P-end-labelled lysyl tRNAs with lysyl tRNA synthetase, products were analyzed on 20% acrylamide 7·0 M urea gel. Autoradiogram of such an experiment showed the generation of different fragments of varying sizes. Out of eleven fragments generated, three corresponded to the position of uracil, two to each of dihydrouridine, two to pseudouridine and cytosine and guanine, respectively.

These results clearly indicated that AARS could carry out glycosidase activity on FUra–tRNA resulting in the degradation of FUra–tRNA, thus providing yet another mode of FUra-mediated cytotoxicity.

References

1. Major, P. P., Egan, E., Herrick, D. and Kufe, D. W. *Cancer Res.*, 1982, **42**, 3005–3009.

2. Armstrong, R. D., Takimoto, C. H. and Cadman, E. C *J. Biol Chem.*, 1986, **261**, 21–24.

3	IWATA, T , WATANABE, T AND KUFE, D. W	*Biochemistry*, 1986, **25**, 2703–2707
4	HADJIOLAVA, K. V., NAYDENOVA, Z. G , AND HADJIOLOV, A A	*Biochem Pharmac* , 1981, **30**, 1861–1863
5	NAYAK, R. *et al*	*Proc. Am Assoc. Cancer Res.*, 1980, **21**, 30.
6	ZUBAY, G.	*J. Mol. Biol* , 1962, **4**, 347–356.
7.	KUMAR, A. M AND NAYAK, R	*Biochem Biophys Res. Commun.*, 1988, **152**, 593–597
8.	DANG, C V. AND YANG, D. C. H	*Biochem Biophys Res Commun* , 1978, **80**, 709–714.

Thesis Abstract (Ph.D.)

X-ray diffraction studies on belladonna mottle virus at 3·8 Å resolution by Chaitanya N. Hiremath.
Research supervisor: Mathur R. N. Murthy.
Department: Molecular Biophysics Unit.

1. Introduction

Tymoviruses are a group of highly infectious plant viruses found in several geographical locations. The type member of this group of viruses, turnip yellow mosaic virus, has been studied in detail regarding its architecture, stability, assembly and disassembly. The early studies on this virus were instrumental in the elucidation of physicochemical principles underlying biological assembly of highly symmetrical macromolecules[1]. Although extensive solution low-angle scattering and single-crystal X-ray diffraction studies have been reported on turnip yellow mosaic virus, it is surprising that the three-dimensional structure of none of the tymoviruses has been determined to date. Determination of the three-dimensional structure of a tymovirus will provide the molecular basis required for the rational understanding of the large number of biophysical data available on tymoviruses. Towards this goal, structural studies on a member of the tymovirus group, belladonna mottle virus (BDMV), were undertaken.

2. Purification and crystallization of BDMV

BDMV was propagated on *Nicotiana glutinosa* and purified from infected leaves by differential centrifugation. Empty capsids formed *in vivo* were separated from the particles containing RNA by sucrose density gradient centrifugation. The purified virus was periodically examined by electron microscopy, absorbance measurements, sedimentation properties and SDS gel electrophoresis. Crystals diffracting to slightly better than 4·0 Å resolution were obtained by precipitation of the virus (30–40mg/ml) from 0·1M sodium citrate buffer, pH 5·5 containing 2·5–3·0% (w/v) polyethylene glycol 8000 and 10mM dithiothreitol. Addition of dithiothreitol was essential to protect the crystals from degradation. The crystals were examined using X-rays from a rotating anode X-ray generator. The crystals belong to the rhombohedral space group R3 with $a = 300$ Å and $\alpha = 60°$. The unit cell contains one molecule of the virus particle.

3. X-ray diffraction data collection

Screenless oscillation photography is the method of choice available for recoding X-ray diffraction data from crystals with large unit cells. In rhombohedral R3, data are most efficiently recoded by rotating the crystal about the 3-fold axis[2]. Due to the pseudo-cubic nature of BDMV crystals, certain special precautions had to be undertaken to avoid indexing errors. The crystals were mounted so as to align the rhombohedral [111] direction parallel to the spindle axis. A preliminary 1° oscillation photograph at the spindle setting corresponding to a major zone was recorded and compared with a series of previously recorded 'standard' photographs. This enabled correct identification of the handedness of the photograph. For recording

diffraction data, the oscillation range was set to 0·6–0·8°. The crystal-to-film distance was 100 mm. Of the 95 crystals examined, 48 were found suitable for data collection and a total of 74 A/B pair of photographs were recorded using these crystals. A total of 44·8° of oscillation was performed with an overlap of 0·1° between the neighbouring photographs. The films were digitized on a Joyce Loebl film scanner at 50 μm intervals. The digitized images were processed on a PDP 11/44 system using a computer program originally written by Rossmann[3] and subsequently modified by Rayment and Murthy. An alternative approach for the determination of crystal orientation suggested by Mathews and coworkers[4] was attempted and was found to be less suitable for virus crystals when compared to Rossmann's 'convolution' procedure.

4. Scaling and post-refinement

Reflection files obtained by processing oscillation films were scaled together using the procedure described by Rossmann *et al*[3]. Initially, the 74 pairs of A/B films were scaled together. The R-factors between these pairs varied between 6·2 and 12·8% with a mean value of 9·5%. Subsequently, the reflections on the 74 files obtained after A/B scaling were merged and scaled using a film of intermediate quality as the standard. Both for A/B scaling and pack-to-pack scaling, a linear scale and an isotropic temperature-like factor were refined. After the determination of scale factors, the cell parameters and crystal orientations were refined by the post-refinement procedure, which minimized the RMS difference between the observed and computed partiality of reflections occurring at the edges of lunes. The missetting angles derived from different photographs recorded from the same crystal were in good agreement. A total of 265327 observations were found on the merged file of which 220110 were accepted. The data set contained 385 reflections for which only overloaded measurements were available. The merging R-factor for the 150912 independent reflections was 16·2% which reduced to 12·0% for the 91340 reflections with $I/r(I) \geq 3{\cdot}0$. The final data set with $I/r(I) \geq 1{\cdot}5$ represents 65% of the theoretically possible data to a resolution of 4·0 Å and 74% to 4·5 Å

5. Use of an area detector system for data collection

Various strategies were attempted for collecting and processing low-resolution (7·8 Å) X-ray diffraction data on virus crystals using a Nicolet/Siemens area detector system. Data were collected both on native and derivative crystals of BDMV. Area detector frames were processed assuming a triclinic system and subsequently averaged for rhombohedral equivalents. This strategy could be generally useful for crystals with pseudosymmetry. The area detector native data scaled well with film data and resulted in an R-factor of 12·4% and a correlation coefficient of 0·94.

6. Rotation function studies

The symmetry of the virus particle was established by rotation function studies. The anticipated icosahedral symmetry of the virus particle and the particle orientation in the unit cell had already been determined in an earlier study using 6·0 Å film data[5]. However, redetermination of particle orientation with the higher resolution data collected for the present work and use of a locked rotation function provided better estimates of the directions of particle symmetry axes in the crystal unit cell[6]. Earlier, cross-rotation function studies had suggested that the BDMV structure resembles that of southern bean mosaic virus. The comparison with other viruses indicated an even greater degree of similarity between BDMV and cowpea mosaic virus. These results suggested that the cowpea mosaic virus is probably a better starting model for the determination of the structure of BDMV by molecular replacement technique.

7. Attempts of structure determination

Attempts to determine low-resolution phases by *ab initio* molecular replacement were not successful probably due to the pronounced non-spherical character of BDMV capsid. None of the derivatives tested were found suitable for obtaining reasonably reliable phases for initiating phase refinement by molecular replacement. Some of the problems associated with preparation of the derivatives were traced to the existence of polyamines bound to BDMV RNA and interfering with the cationic heavy atom salts. Hence, attempts were directed at using cowpea mosaic virus as an initial model for BDMV structure. The various strategies

used for phase refinement and a critical assessment of the progress of molecular replacement are presented. The electron density map computed after extending the phases to 4·8 Å resolution was found to be uninterpretable. These results were critically examined to understand the reasons for the quality of the map.

8. Future prospects

Future work on BDMV X-ray structure determination should focus on preparation of heavy atom derivatives using crystals produced after replacing polyamines by inorganic cations, exploring conditions for producing crystals that diffract to near atomic resolution and combined studies on BDMV and erysimum latent virus, which is also a tymovirus. These studies will reveal similarities and differences between tymoviruses and other spherical viruses and finer details of tymoviral architecture and evolution.

References

1. MURTHY, M. R. N., HIREMATH, C. N. AND SAVITHRI, H S. — In *Molecular conformation and biological interactions* (P. Balaram and S Ramaseshan, eds), 1991, Indian Academy of Sciences, Bangalore
2. MUNSHI, S K. AND MURTHY, M. R. N — *J Appl. Crystallogr*, 1986, **19**, 61–62.
3. ROSSMANN, M. G , LESLIE, A. G. W., ABDEL-MEGUID, S. S. AND TSUKIHARA, T. — *J. Appl. Crystallogr.*, 1979, **12**, 570–581.
4. SCHMID, M. F , WEAVER, L. H , HOLMES, M. A., GRUTTER, M G., OHLENDORF, D. H., RAYNOLDS, R. A., REMINGTON, S. T. AND MATTHEWS, B. W. — *Acta Crystallogr. B*, 1981, **37**, 701–710
5. MUNSHI, S K., HIREMATH, C. N., SAVITHRI, H. S. AND MURTHY, M R. N. — *Acta Crystallogr. B*, 1987, **43**, 376–382.
6. HIREMATH, C. N., MUNSHI, S K. AND MURTHY, M. R. N. — *Acta Crystallogr. B*, 1990, **46**, 562–567.

Thesis Abstract (Ph.D.)

The gene for the major antigenic protein of foot and mouth disease virus, Type Asia 1 63/72 by V. V. S. Suryanarayana.
Research supervisors: J. D. Padayatty, T. Ramasarma and B.V. Rao (Orgn).
Department: Biochemistry.

1. Introduction

Foot and mouth disease virus (FMDV) contains a positive-sense single-strand RNA enclosed in a protein capsid composed of four structural proteins, VP1, VP2, VP3, and VP4[1]. VP1 is the major antigenic protein and the variations in this protein resulted in the occurrence of seven serotypes and over sixty subtypes of the virus[2]. India is a habitat for the four serotypes, O, A, C and Asia I. The serotypes O, A and C are subjected to intensive studies to develop cost-effective and safer immunogens and to understand the molecular basis of antigenic variations. To understand the variations and to develop vaccine against Asia I virus, an isoalte, 63/72, of the serotype Asia 1 was investigated.

2. Methodology and preparation of antigenic proteins

Double-stranded cDNA for the viral RNA was synthesized and inserted at the *Pst*I site in the vector pUR222[3] by dC/dG tailing method, transferred into *E. coli* BRI TΔ5 and grown on 5-bromo-4-chloro-3-indolyl β-D-galactopyranoside and isopropyl β-thio galactopyranoside agar plates. The presence of the insert in the colourless colonies was detected by colony hybridization with ^{32}p-end labelled FMDV Asia I RNA. Colonies which showed strong hybridization signals were tested for the production of major antigenic protein, VP1, by the enzyme-linked immunosorbant assay (ELISA)[4] using antibodies raised against inactivated virus. The one which gave the strongest reddish brown colour was grown in the presence of ^{35}S-methionine and a protease inhibitor, phenylmethylsulphonylfluoride, the cells were lysed and the labelled proteins were analysed by sodium dodecylsulphate polyacrylamide gel electrophoresis (SDS-PAGE). An additional protein band corresponding to 38 kDa was observed on the autoradiogram from the clone bearing the insert cDNA.

The labelled proteins were immunoprecipitated with monoclonal antibodies, antibodies raised agianst the purified VP1 and inactivated virus and analysed by SDS-PAGE. A band corresponding to 20 kDa, in addition to a band corresponding to 38 kDa was observed on the autoradiogram. The presence of major antigenic epitopes of VP1 on the 38 and 20 kDa proteins was confirmed by competitive ELISA, radioimmunoassay and plaque-inhibition assay. The immunoprecipitates of proteins using antibodies raised against the proteins present in the lysate showed the presence of an 18 kDa protein in addition to the 38 and 20 kDa antigenic proteins. The primary product of the cloned cDNA may be the 38 kDa protein which on proteolysis results in 20 and 18 kDa proteins.

3. Results and conclusions

The proteins produced by the cloned cDNA were highly immunogenic in guinea pigs and cattle. With a single injection of 100 μg of the protein which is equivalent to 4 μg of the VP1, in guinea pigs, the serum antibody titers increased by 16–32 fold as determined by virus neutralization assay. A single injection of 10–20 μg of the protein protected five of the eight guinea pigs against challenge by the injection of a 100 guinea pig ID_{50} of the virulent Asia I virus. On injecting the protein from the lysate to eight male cattle (3 mg protein equivalent to 120 μg of the immunogen on days 0 and 28) the antibody levels in the serum of the animals increased 100 fold within 40 days. Three of these immunised animals were completely protected when challenged with 10,000 cattle ID_{50} of the virulent Asia I virus.

The size of the inserted cDNA coding for the antigenic protein was 0·9 kb. The sites for *Pst*I and *Sal*I are present on the insert DNA, while the *Bam*H1, *Hind*III, *Eco*RI, *Bgl*II, *Kpn*I, *Sac*I and *Hin*fI sites are absent. Different restriction fragments of the insert DNA were cloned in the phage M13mP11 or M13mp19, the recombinant phages were grown, the single-stranded DNAs were prepared and sequenced by the dideoxy chain termination method[5]. A sequence of 879 nucleotides was obtained from the overlapping sequences. The *Sal*I site and *Pst*I sites are located at 483 and 733 nucleotides downstream from 5′ end. The nucleotide sequence was aligned using a computer programme GAP with the known nucleotide sequence of VP1 gene of different strains of FMDV and was found to have a maximum homology with that of the C_3 virus to the extent of 40 per cent. The inserted DNA is of 65 per cent GC rich and does not contain signal and site for initiation of transcription and translation. The cloned DNA was expressed by using the lac promoter and ATG codon of the α-complementation protein of β-galactosidase present on the vector. The inserted DNA sequence is in frame with the nucleotide sequence corresponding to five amino acids of the α-complementation protein, starting from AUG. A sequence of 293 amino acids was derived from the nucleotide sequence. The molecular weight of the derived protein was estimated to be 31·6 kDa. Together with the five amino acids of 0·57 kDa at the N-terminus and 55 amino acids of 6·05 kDa at the C-terminus of the α-complementation protein, the expressed protein is of 38·2 kDa. This agrees well with the 38 kDa size of the immunogenic protein produced by the cloned cDNA. There are 43 arginine, 4 lysine, 7 glutamic acid and 18 aspartic acid residues in the derived amino acid sequence making the protein highly basic which is in agreement with the highly basic nature of the 38 kDa protein. The cloned cDNA may be used as a probe for serotyping FMDV and production of a vaccine against the FMDV, Asia I 63/72.

References

1 BACHRACH, H. L — In *Proc. Beltsville Symposia in Agricultural Research–Virology in Agriculture*, 1977, Allanheld, Osmun and Co., Montlhair, N J (Romberger, J. A , ed.), pp 3–22.

2. ROWLANDS, D. J., CLARKE, B. E , CARROLL, A. R., BROWN, F., NICHOLSON, B. H , BITTLE, J. L., HOUGHTEN, R. A. AND LERNER, R A. — *Nature*, 1983, **306**, 694–697.

3. RUTHER, U., KOENEN, M , OTTO, K. AND MULLER HILL, B — *Nucleic Acids Res.*, 1981, **9**, 4087–4098.

4 ABU-ELZEIN, E. M. E. AND CROWTHER, J R — *J. Hyg.*, 1978, **80**, 391–400

5. SANGER, F., NICKLEN, S AND COULSON, A. R. — *Proc Natn Acad. Sci.*, 1977, **14**, 5463–5467.

Thesis Abstract (Ph.D.)

Carbohydrate binding analysis, primary structure and structure–function correlationship of *Artocarpus integrifolia* agglutinin, Jacalin by Sanjeev Kumar Mahanta.
Research supervisor: Avadhesha Surolia.
Department: Molecular Biophysics Unit.

1. Introduction

Lectins, first discovered in 1888, are a class of proteins with carbohydrate-binding and cell-agglutinating properties. Their binding to cell surface carbohydrates confer upon them interesting biological properties that in some cases include blood group-specific recognition and mitogenic stimulation of lymphocytes. Crude seed extract of *Artocarpus integrifolia* (jackfruit) contains a lectin with many interesting biological properties. Initial studies suggested that this lectin, jacalin, might recognize the immunodominant carbohydrate portion of Thomsen–Friedenreich antigen (T-antigen), a chemically well-defined antigen associated with certain types of cancer. T-antigen being an important carcinoma marker, anti-T probes are useful as diagnostic reagents. Hence, a detailed carbohydrate-binding analysis of jacalin was carried out in the past[1]. The studies reported here further characterize its interaction with sugar and reveal certain unique features of its carbohydrate specificity. In addition, circular dichroism spectroscopic studies carried out on ligand binding to jacalin provide information on the probable mode of arrangement of saccharides in the lectin-combining region.

To correlate the binding behaviour of jacalin with its structure, the complete amino acid sequence of the lectin has been determined by manual Edman degradation. The protein was found to be composed of heavy and light chains and the heavy chain showed the presence of an internal repeat spanning over 90% of the sequence. Chemical modification studies that followed sequence determination underlined the importance of lysine residues for antigenicity and carbohydrate binding. Also, these studies led to the identification of a peptide segment of jacalin heavy chain of strongly antigenic nature, and that of a lysine residue involved in carbohydrate binding and antigenicity.

2. Experimental

Jacalin used for all studies was purified by affinity chromatography on crosslinked guar gum. Ligand-induced changes in the intrinsic fluorescence intensity of jacalin upon binding to sugars were used to derive the various parameters of association. Changes in the circular dichroism (c.d.) spectra of jacalin upon interaction with sugars were monitored in the wavelength region between 250 and 300 nm. Quantification

of the association of oligosaccharides with peanut agglutinin (PNA) was performed by substitution titration using fluorescence spectroscopy and N-dansylgalactosamine as the extrinsic probe.

The constituent subunits of jacalin were purified by a combination of gel filtration and reverse-phase high-performance liquid chromatography (r.p.h.p.l.c.). The heterogeneity of jacalin was characterized by chromatofocussing and isoelectric focussing. Chemical cleavages using CNBr, hydroxylamine hydrochloride, and iodosobenzoic acid, and enzymatic cleavage using *Staphylococcus aureus* V8 protease were used to generate fragments of jacalin heavy chain suitable for sequencing. Peptide fragments were purified by gel filtration and reverse-phase fast-protein liquid chromatography (r.p.f.p.l.c.). Sequence determination was carried out by manual Edman degradation using 4-dimethylaminoazobenzene 4'-isothiocyanate (DABITC) as the coupling reagent. The sequence comparison programme PLFASTA was used to detect the presence of internal repeat in jacalin heavy chain.

Chemical modification studies were carried out by modifying lysine residues of the protein in the presence and absence of sugar. Antigenicity of the protein and peptides was checked with Ouchterlony double diffusion and ELISA.

3. Results and discussion

This study provides several important information on the sugar specificity of jacalin[2]. For instance, despite its strong affinity for MeαGal and MeαGalNAc, the lectin reacts very poorly when Gal and GalNAc are in α-linkage with other sugars as in A- and B-blood group trisaccharides. It binds Galβ1, 3GalNAcαMe with over 2500-fold higher affinity as compared to Galβ1, 3GalNacβMe and does not bind asialo G_{M1} oligosaccharide. In this respect it surpasses the ability of peanut lectin and several anti-T monoclonals which discriminate poorly between the α- and β-linked T-antigenic structures. These results indicate that jacalin should complement the existing anti-T probes for monitoring the expression of T-antigen on cell surfaces. Ligand-structure-dependent alterations of the c.d. spectrum in the tertiary structural region of the protein suggest a possible mode of arrangement of various sugar units in the combining region of the lectin[2]. It appears that the primary subsite (subsite A) can accommodate only Gal or GalNAc or α-linked Gal or GalNAc, whereas the secondary subsite (subsite B) can associate with either GalNAcβMe or Galβ Me.

Carbohydrate binding analysis of peanut lectin showed that it discriminates poorly between the α and β glycosides of the T-antigenic disaccharide[3]. Thus, unlike jacalin, it has a high affinity for asialo-G_{M1} tetrasaccharide, which has Galβ1, 3GalNAc in β-linkage to the remaining saccharide portion. Moreover, the subsite specificity of PNA appears to be the reverse of that of PNA.

Isoelectric focussing of jacalin shows a smear-like pattern in the pH range 6·5 to 8·6, thereby underlining the excessive microheterogeneity of the protein[4]. The use of chromatofocussing also provides evidence for the unusually high level of heterogeneity. A combination of gel filtration, r.p.h.p.l.c. and N-terminal sequence analysis provided evidence for the presence of two types of polypeptides, the heavy and the light chain, as the constituent polypeptides of jacalin.

Complete sequence determination of jacalin showed that the heavy chain is made up of 133 amino acids, whereas the light chains are only 20 residues in length[4]. Its heavy chain shows the presence of an internal repeat spanning over 90% of the sequence, which in all likelihood encompasses the residues involved in carbohydrate recognition. Therefore, the internal repeat is an important structural feature and is possibly of direct relevance to its carbohydrate binding[4].

Jacalin heavy chain when subjected to standard theoretical analysis revealed the presence of a nine-residue stretch with high values of antigenicity index and surface probability. ELISA and competitive ELISA with a small peptide containing this nine-residue stretch provided evidence for the strongly antigenic nature of this peptide. Chemical modification of lysine residues, known to abolish the carbohydrate binding of jacalin was also found to lead to a loss of recognition by anti-jacalin antiserum. Furthermore, it was found that protection of lysine residues from being modified by the presence of sugar led to retention of carbohydrate binding as well as antigenicity. The nine-residue antigenic peptide described above contained

three lysine residues. Therefore, these lysine residues were checked for their involvement in antigenicity and carbohydrate binding, and results pointed towards Lys-90 as being a residue essential for saccharide binding and important for recognition by antiserum. These studies have thus laid the groundwork for future structure–function correlationship studies on jacalin.

References

1. SASTRY, M. V. K., BANERJEE, P., PATANJALI, S. R., SWAMY, M. J., SWARNALATHA, G. V AND SUROLIA, A. — *J. Biol. Chem.*, 1986, **261**, 11726–11733.
2. MAHANTA, S. K., SASTRY, M. V. K. AND SUROLIA, A. — *Biochem. J.*, 1990, **265**, 831–840.
3. SWAMY, M. J., GUPTA, D., MAHANTA, S. K. AND SUROLIA, A. — *Carbohyd. Res.*, 1991, **213**, 59–67.
4. MAHANTA, S. K., SANKER, S., PRASAD RAO, N. V. S. A. V., SWAMY, M. J. AND SUROLIA, A. — *Biochem. J.*, 1992, **284**, 95–101.

Thesis Abstract (Ph.D.)

Social biology of the tropical primitively eusocial wasp *Ropalidia marginata* (Lep.) **(Hymenoptera: Vespidae)** by K. Chandrashekara.
Research supervisor: Raghavendra Gadagkar.
Department: Centre for Ecological Sciences.

1. Introduction

Ropalidia, a genus of the primitively eusocial polistine wasps, well known for its diversity of nesting biology and social organisation has been the subject of several studies in recent years[1–3]. Our understanding of the biology and social organisation of *Ropalidia*, however, is still in its infancy[1]. The objective of this study, therefore, was to further our understanding of division of labour and social organisation in *Ropalidia marginata* and attempt to throw some light on the question of the origin and evolution of social life.

2. Correlates of behavioural castes and dominance

There is considerable inter-individual variability in the behaviour of wasps in a colony of *R. marginata* and a multivariate statistical analysis of this variability can be used to identify three behavioural groups, namely, Sitters, Fighters and Foragers which may be termed behavioural castes[1]. In the present study, I examined behavioural, morphological and anatomical correlates of such behavioural castes in 12 post-emergence colonies to establish the role of behavioural caste differentiation in the division of labour and social organisation in *R. marginata*. My results show that the Foragers were primarily responsible for the risky task of foraging and had the most poorly developed ovaries. On the other hand, intra-nidal tasks such as feeding larvae and nest-building were shared by Sitters and Fighters, who foraged rarely, if at all. Fighters also showed dominance significantly more often than either Sitters or Foragers. Both Sitters and Fighters had better developed ovaries compared to the Foragers, but the behavioural castes were morphologically indistinguishable. Each colony had a single egg-layer (queen) who in 11 out of 12 colonies was in the Sitter caste. The queen often did not participate in dominance interactions and even when she did, she was not necessarily at the top of the behavioural dominance hierarchy of her colony. Thus, division of labour and social organisation are achieved through behavioural caste differentiation and not through a despotic queen suppressing all her nestmates into worker roles. I argue that this is a consequence of behaviour patterns being moulded by an interaction of selection at the individual and colony levels.

3. Unmated females as queens

In 5 out of 11 colonies (in one colony the queen could not be dissected) the queen was unmated even though in two colonies there was at least one mated female. A typical caste differentiation into Sitters and Foragers was seen in all colonies, whether or not their queens were mated, reflecting normal social organisation. A comparison of colonies with mated queens and those with unmated queens using a number of variables failed to establish any quantitative differences between the two types of colonies. I conclude therefore that mating is not essential for the development of a female's ovary and that unmated females can become queens, prevent their nestmates from laying eggs and maintain normal social organisation I argue that in species such as *R. marginata*, where intra-colony relatedness is expected to be low and where sociality is likely to be maintained because several individuals have opportunities for direct reproduction in the future (see below), individual selection may sometimes override 'the good of the colony' and lead to such phenomena as that of unmated queens.

4. Nesting cycle and serial polygyny

I monitored two post-emergence colonies for 10 and 22 months, respectively, and found that the nesting cycle consists of several repeats of the typical determinate cycle observed in other species. At the end of each unit of the colony cycle, most of the brood and cells were destroyed and a large proportion of the adults left the nest. A sub-set of the females, with or without the same queen, however, often continued on the same nest. In colonies of *R. marginata*, there is strict monogyny at any given time; however, frequent queen replacements over time led to serial polygyny[4]. Queen replacements in *R. marginata* did not seem to follow any seasonal pattern, nor were the nests deserted following queen replacements. In fact, the workers continued to stay back on the nest and bring up offspring of several matrilines. New queens were found to be daughters, sisters, nieces or cousins of their predecessor queens and workers were thus found to rear brood who ranged from their full-sisters ($r = 0.75$) to their mother's cousin's grand offspring ($r = 0{\cdot}0234$). These data reinforce the idea that genetic asymmetry created by haplodiploidy is unlikely to be a significant factor in selecting for worker behaviour in such species[4].

5. Queen succession

The perennial indeterminate nesting cycle and the phenomenon of serial polygyny often provides opportunities for workers in a colony to become queens[4]. What kind of individuals become queens when the original queen dies or is removed? The results from queen removal experiments show that potential queens are usually either Sitters or Fighters and are neither the most dominant individuals nor the oldest individuals in their colonies. These results appear radically different from the so-called temperate pattern where old active foragers are potential queens and consistent with the so-called tropical pattern where relatively young non-foragers are potential queens. However, it may be more appropriate to describe the potential queens of *R. marginata* as 'unspecialised intermediates' who may be able to quickly respond to the loss of a queen and replace her.

6. Conclusions

These results, taken together with previous data on *R. marginata*, especially those demonstrating multiple mating by queens and the probable absence of the ability to discriminate different levels of genetic relatedness within a colony, suggest that mutualistic interactions among potential reproductives may be more important than the genetic asymmetry created by haplodiploidy in selecting for worker behaviour[3,5].

References

1. GADAGKAR, R. AND JOSHI, N. V. — *Anim. Behav.*, 1983, **31**, 26–31.
2. KOJIMA, J. — *Insectes Sociaux*, 1989, **36**, 197–218.
3. GADAGKAR, R. — In *Social biology of wasps*, (K. G. Ross and R. W. Matthews, eds), 1991, pp 149–190, Cornell Univ. Press, NY.
4. GADAGKAR, R., CHANDRASHEKARA, K, CHANDRAN, S. AND BHAGAVAN, S. — *Naturwissenschaften*, 1991, **78**, 523–526.
5. LIN, N. AND MICHENER, C. D. — *Q. Rev. Biol*, 1972, **47**, 131–159.

Thesis Abstract (Ph.D.)

Regulation of the respiratory function of brown adipose tissue mitochondria by Amos Gaikwad.
Research supervisors: C. K. R. Kurup and T. Ramasarma.
Department: Biochemistry.

1. Introduction

Brown adipose tissue (BAT) is believed to play an important role in nonshivering thermogenesis based on its ability to show rapid responses to thermogenic conditions. The discovery of the uncoupling protein (UCP) and the elucidation of its role as a purine nucleotide regulated, proton-translocating uncoupler protein led to the concept that the thermogenic function of BAT was regulated by UCP. The aim of this investigation was to understand the rapid regulation of BAT mitochondrial electron transport in response to sudden changes in environmental temperature.

2. Experimental procedure

The simple procedure of exposing cold-acclimated (4°C, 30 days) animals to high temperature (37°C; 3 and 12 h) was used to evaluate the changes occurring about the same time span for normalization of basal metabolic rate (BMR) to study this phenomenon As the experimental protocol consists of a large temperature differential (4°C to 37°C), one expected rapid changes to occur in those reactions participating in thermogenesis. The studies include the changes occurring in BAT mitochondria (oxidative and UCP-related activities) and in the concentration of hormones (T_3, T_4 and insulin) in the tissue and in circulation. During the course of this investigation, it was found that BAT mitochondria are cytochrome *c* subsaturated.

3. Results

Exposure of rats to the cold caused large (2–3 fold) increases in the mass of interscapular BAT, its mitochondrial content and in the BMR of the animals. The rate of substrate oxidation by BAT mitochondria also increased about 3 fold (Fig. 1). When cold-acclimated animals were exposed to heat (37°C), the BMR decreased by half in 3 h, the earliest time interval tested (Fig. 1). Mitochondrial substrate oxidation as well as substrate-dependent H_2O_2 generation showed proportionate decrease in rates. The concentrations of cytochromes *aa* and *b*, but not of cytochrome *c* also decreased in BAT mitochondria from 12 h heat-exposed animals. The concentration of cytochrome *b* (Table I) and its rate of reduction alone was found to decrease as early as 3 h of heat exposure (Fig. 2). These results suggest that cytochrome *b* may play a key role in the rapid regulation of electron transport in BAT mitochondria under conditions of acute heat stress.

Some parameters such as the UCP concentration, GDP binding and swelling capacity of mitochondria in BAT are considered to be thermogenic markers. Significant changes in these parameters have been observed and correlated with the thermogenic status of the animal. A significant decrease in the GDP binding, without a decrease in UCP concentration, was found in BAT mitochondria as early as 3 h of heat exposure. The swelling capacity, a marker of the degree of proton conductance, also showed a significant decrease. After 12 h of heat exposure the concentration of UCP as well as the purine nucleotide-binding capacity of mitochondria showed about 50% decrease. The concentration of GDP required to inhibit oxidative activity of BAT mitochondria increased by 1·3 fold on 12 h of heat exposure.

Noradrenaline and thyroid hormones exert a synergestic action on BAT.

Acclimation of rats to the cold caused a 45% increase in the concentration of triiodothyronine (T_3) and a 35% increase in the concentration of thyroxine (T_4) in serum. Short-term heat exposure failed to decrease the concentrations of thyroid hormones in circulation. The concentration of T_3 in BAT increased almost 10 fold on cold acclimation. Iodothyronine deiodinase activity also registered a 3-fold increase. Heat exposure caused a decrease in the concentration of T_3 in BAT without appreciably affecting T_4 concentration. On thryoidectomy or when fed with propylthiouracil, rats could not survive exposure to the cold, in spite of the increased BAT mass. The concentration of insulin in circulation showed a small increase while that in the

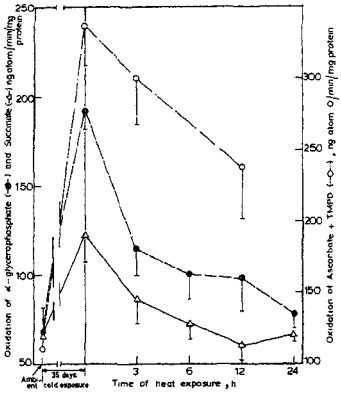

FIG. 1. Effect of exposure of the rat to cold and heat on the oxidative activity of BAT mitochondria. Cold-acclimated rats (5°C, 35 days) were exposed to heat (37° C) for the time periods indicated. BAT mitochondria isolated from animals kept at ambient temperature, cold-acclimated and heat-exposed were assayed for the oxidation of α-glycerophosphate (-- ● --), succinate (—▲—) and ascorbate + TMPD (--○--). The rates of substrate oxidation by BAT mitochondria obtained from animals kept at ambient temperature exposed to cold for 35 days and shifted to heat (37°C) for the time intervals (h) induced. The values are the mean of six independent samples. The mean ± S.D. is given.

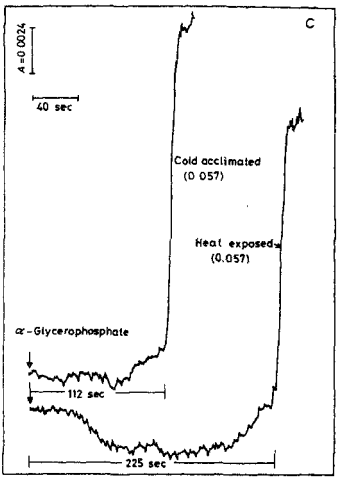

FIG. 2 Effect of exposure of cold-acclimated rats to heat on the rate of reduction of cytochrome *b* in BAT mitochondria. Substrate (α-glycerophosphate)-dependent reduction of cytochrome *b* in BAT mitochondria isolated after 12 h of exposure of animals to heat (37° C) and from cold-acclimated animals was followed at 562–575nm in a dual wavelength spectrophotometer: The system contained the same amount of mitochondria (1 mg) in ml. The time for the onset of anaerobiosis on addition of substrate is indicated. The numbers in the parenthesis indicate the increase in the rate absorbance at the onset of anaerobiosis expressed as absorbance at the onset of anaerobiosis expressed as absorbance change/min per mg mitochondrial protein.

tissue showed a significant decrease during cold acclimation. The concentration of the hormone in BAT registered a significant increase on short-term heat exposure. The temperature-dependent response of T_3 and insulin indicates an important role for these hormones in rapid physiological response in BAT.

During the course of this investigation, it was found that the oxidative activity of freshly isolated BAT mitochondria was stimulated two fold on exogenous addition of cytochrome *c*. Maximal stimulation was obtained at 8 μM cytochrome *c* concentration. Loss of membrane-bound cytochrome *c* did not occur during isolation of mitochondria. Estimation of the high-affinity binding sites on the organelle membrane indicated that less than a third of these sites remained saturated with cytochrome *c*. The pigment is thus shown to be a functionally limiting electron-transport component.

4. Conclusion

The data suggest cytochrome *b* as the focal point in rapid regulation of the respiratory chain activity in

Table I

Effect of exposure of cold-acclimated animals to heat on the cytochrome and ubiquinone content of BAT

Cold-acclimated animals were exposed to heat (37°C) for the time periods indicated The cytochrome content of BAT mitochondria was calculated from difference spectra and in the tissue by pyridine hemochrome formation The ubiquinone content in BAT was measured by absorbance change at 275 nm on addition of $NaBH_4$ to non-saponifiable lipids. The values given are mean ± S.D of independent determinations (sample number : cytochrome by difference spectra, 10–13; cytochromes by pyridine hemochrome, 3; ubiquinone, 3–5).* $P < 0.05$, **$P < 0.01$, heat-exposed *vs* cold-acclimated

Component	*Cold-acclimated*	*Heat exposed*	
		3 h	*12 h*
Cytochrome (pmol/mg mit. protein)			
aa_3	492 ± 47	513 ± 8	369 ± 63**
b	487 ± 59	369 ± 36**	343 ± 34**
c	497 ± 81	451 ± 16	466 ± 88
Cytochrome (nmole/g BAT)			
aa_3	16 ± 20	–	12 ± 2·0*
b	14 ± 0·3	–	10 ± 1·0**
c	19 ± 2·0	–	18 ± 3·0
Ubiquinone (nmol/g BAT)	175 ± 27	–	176 ± 15

BAT mitochondria when cold-acclimated rats are shifted to hot environment (37°C, 3 h). The content as well as the rate of reduction of this radox component was significantly decreased as early as 3 h of heat exposure. During 12 h heat exposure of cold-acclimated rats, the other non-covalently bound hemoprotein, cytochrome *aa* also showed a significant decrease in concentration. The serendipitous discovery that BAT mitochondria are cytochrome *c* subsaturated and remain so under all physiological conditions is intriguing. The extraordinarily large concentration of cytochrome *c*-binding sites in BAT mitochondria is possibly a reflection of the high content of acidic lipids such as phosphatidyl ethanolamine and cardiolipin which are known to influence the binding of cytochromes to mitochondrial inner membranes.

References

1. Amos Gaikwad, Ramasarma, T. and Kurup, C. K. R — *Biochem. Biophys. Acta*, 1990, **1017**, 242–250.
2. Amos Gaikwad, Ramasarma, T. and Kurup, C. K. R. — *Indian J. Biochem. Biophys.*, 1990, **27**, 167–171.
3. Amos Gaikwad, Ramasarma, T. and Kurup, C. K. R. — *Mol. Cell. Biochem.*, 1991, **105**, 119–125.

Thesis Abstract (Ph.D.)

Biochemical and physiological effects of methyl isocyanate in mammals by K. Jeevaratnam. Research supervisors: C. S. Vaidyanathan and R. V. Swamy*. Department: Biochemistry.

1. Introduction

Methyl isocyanate (MIC) is used primarily as a chemical intermediate in the manufacture of methylcarba-

* Defence Research and Development Establishment, Gwalior

mate insecticides, polyurethane foams, plastics and certain pharmaceuticals[1]. It is the major culprit in the Bhopal gas tragedy due to the release of a poisonous cloud from the Union Carbide pesticide plant on the night of December 2/3, 1984. MIC is a liquid at room temperature and pressure, but highly volatile with a vapour pressure of 348 mm Hg at 20°C It is soluble in water and also reacts with water to form methylamine and N, N'-dimethylurea. It is highly reactive molecule, reacts with functional groups such as amino, hydroxyl, sulfhydryl, etc[2] One of the striking features of Bhopal disaster in which several thousand people lost their lives was the lack of toxicological information on the major causal agent, MIC. The only pertinent study available prior to the worst chemical disaster is that of Kimmerle and Eben[3] who established that MIC is highly irritating to skin and mucosae and concluded from gross necropsy findings that inhaled MIC causes pulmonary edema. MIC being a potent sensory and pulmonary irritant affects primarily the respiratory system in rodents[4,5]. In this work, the acute toxicity of MIC was studied with special reference to MIC-induced biochemical and physiological changes in mammals in order to delineate the mechanisms involved leading to severe tissue hypoxia, respiratory failure and death.

2. Results and discussion

Firstly, the acute LC_{50} (inhalation route) LD_{50} (subcutaneous route) of MIC were determined. Various concentrations, 0·5, 1·0, 2·0 LC_{50} of MIC and doses 0·5, 1·0, 2·0 LD_{50} of MIC were used to elucidate its hematological and biochemical effects in rats. Irrespective of the route of administration of MIC the hematological and biochemical changes such as hemoconcentration, increased plasma total proteins with decreased plasma albumin, hyperglycemia, severe lactic acidosis and uremia are dose-related and quite similar in rats except for the variation in the intensity of the effects[6]. These hematological and biochemical changes were also essentially similar in rabbits[7], a non-rodent reflecting the species similarity of systemic toxic effects of MIC in mammals. The observed hematological and biochemical changes were mostly due to MIC *per se* in spite of its hydrolytic instability because of the failure of its hydrolysis products, methylamine (MA) and N, N'-dimethylurea (DMU) to influence these parameters in both the species of mammals[8].

MIC was found to carbamylate N-terminal amino group of hemoglobin *in vivo*. However, in contrast to the earlier report[9], MIC interaction with normal hemoglobin does not seem to alter its quaternary structure and function and does not play a role in the production of tissue hypoxia[10].

The sequence of events occurred with the progress of time after subcutaneous administration of MIC in rabbits clearly indicated the primary event to be hypotension due to MIC-induced generalised vasodilatation which persisted for a longer duration with increasing severity possibly due to fluid loss (hypovolemia). The data on acid-base status of blood such as the decrease in arterial pH, pCO_2, pO_2 and the progressive increase in the difference between arterial and venous oxygen content after MIC intoxication clearly demonstrated that MIC produced severe hypoxia of the stagnant type, acute metabolic acidosis and a decrease in ventricular function and peripheral resistance resulting in hypotension and shock-like condition[11].

The effects of MIC on tissue respiration were investigated by studying the adverse effects of MIC on rat liver mitochondrial respiration both *in vitro* and *in vivo*. MIC stimulated 'state 4' respiration, decreased ADP/O ratio, inhibited 'state 3' oxidation and abolished respiratory control *in vitro* in isolated rat liver mitochondria indicating its action as an 'inhibitory uncoupler'. The oxidation of NAD^+-linked substrates (glutamate + malate) was more sensitive to the inhibitory action of MIC than was of succinate. Apart from inhibiting the electron transport at complex I region, MIC also interfered with the process of translocation of reducing equivalents, NADH into the mitochondria by inhibiting the membrane-bound -glycerophosphate dehydrogenase. MIC also stimulated the dormant ATPase activity in tightly coupled mitochondria. In agreement with the *in vitro* observations, MIC also stimulated the dormant ATPase activity in tightly coupled mitochondria. In agreement with the *in vitro* observations, MIC administered s.c. at lethal dose (1·0 LD_{50}) in rats produced similar effects with glutamate + malate but not with succinate indicating the impairment of electron transport and energy transduction at complex I region of the isolated liver mithochondria from rats intoxicated with MIC compared to the control group. These results clearly showed that MIC did produce histotoxic hypoxia, *in vivo*, when the animals were exposed to lethal doses.

MIC interaction with erythrocyte membrane caused an increased fluidity of the membrane and decreased the osmotic fragility of erythrocytes both *in vitro* incubation and *in vivo* in rabbits intoxicated with MIC subcutaneously, while the erythrocytes become more fragile on subcutaneous administration of its hydrolysis products MIC inhibited both erythrocyte AChE and ATPase enzyme activities *in vitro*, but failed to alter their activities *in vivo* in rabbits administered 1·0 LD_{50} MIC s.c. However, subcutaneous administration of MIC caused significant decrease in plasma Na^+ level and increase in plasma K^+ level in rabbits. The inhibition of Na^+–K^+ ATPase with altered permeability to cations and also probably water transport of the plasma membrane due to MIC interaction with plasma membrane of the vasculature are envisaged[12].

Finally, the observed histological changes in lungs such as severe interseptal edema, collection of fluid and exuded plasma proteins within the interstitial and alveolar spaces and those observed in other vital organs provided clear evidence for the occurrence of fluid loss from the vascular compartment leading to hypovolemic shock as a result of MIC intoxication.

References

1. ANON — India's chemical tragedy: Death toll at Bhopal still rising, *Chem. Engng News*, 1984, **62**, 6–8
2. DODD, D. E. — Toxicology of methyl isocyanate, *Rev. Environ. Contam. Toxicol.*, 1988, **105**, 71–98.
3. KIMMERLE, G. AND EBEN, A. — Zur toxicitat von methyl isocyanat und quantitiver bestimung in der luft, *Arch. Toxicol*, 1964, **20**, 235–241.
4. FERGUSON, J. S., SCHAPER, M., STOCK, M. F., WEVEL, D. A. AND ALARIE, Y. — Sensory and pulmonary irritation with exposure to methyl isocyanate, *Toxicol. Appl. Pharmacol*, 1986, **82**, 329–335.
5. NEMERY, B., DINSDALE, D., SPARROW, S., AND RAY, D. E. — Effects of methyl isocyanate on the respiratory tract of rats, *Br. J. Ind. Med*, 1985, **42**, 799–805
6. JEEVARATNAM, K., VIJAYARAGHAVAN, R., KAUSHIK, M. P. AND VAIDYANATHAN, C. S. — Acute toxicity of methyl isocyanate in mammals: II. Induction of hyperglycemia, lactic acidosis, uraemia and hypothermia in rats, *Arch. Environ. Contam Toxicol.*, 1990, **19**, 314–318.
7. JEEVARATNAM, K., BHATTACHARYA, R., SUGENDRAN, K., AND VAIDYANATHAN, C. S. — Acute toxicity of methyl isocyanate in mammals· IV. Biochemical and hematological changes in rabbits, *Biomed. Environ Sci*, 1991, **4**, 384–391.
8. JEEVARATNAM, K., SUGENDRAN, K. AND VAIDYANATHAN, C. S. — Influence of methylamine and N,N'–dimethylurea, the hydrolysis products of methyl isocyanate on its systemic toxicity, *J Appl. Toxicol.*, 1992 (In press)
9. LEE, C. K. — Methyl isocyanate as an anti-sickling agent and its reaction with hemoglobin S, *J. Biol. Chem.*, 1976, **251**, 6226–6231
10. JEEVARATNAM, K. AND VAIDYNATHAN, C. S. — Does methyl isocyanate interaction with normal hemoglobin alter its structure and function?, *Bull. Environ Contam. Toxicol*, 1992, **48**, 77–82.
11. JEEVARATNAM, K., SELVAMURTHY, W. S. RAY, U. S., MUKHOPADHYAY, S. AND THAKUR, L. — Acute toxicity of methyl isocyanate, administered subcutaneously in rabbits: Changes in physiological, clinico-chemical and histological parameters, *Toxicology*, 1988, **51**, 223–240.
12. JEEVARATNAM, K. AND VAIDYANATHAN, C. S. — Acute toxicity of methyl isocyanate in rabbit: *In vitro* and *in vivo* effects on erythrocyte membrane, *Arch. Environ. Contam. Toxicol.*, 1992 (In press).

IISc Theses Abstracts

AUTHOR INDEX

Jan.–Feb. 1993